Contents lists available at SciOpen

Food Science and Human Wellness

journal homepage: https://www.sciopen.com/journal/2097-0765

China Food Publishing Co.

Targeted metabolomics reveals the role of ginsenoside Rb1 in modulating inflammation and cellular senescence in sepsis-induced acute lung injury

Fushuang Zheng[a,1], Wei Wang[b,1], Linlin Gao[c,*], Zhiling Fu[b,*]

[a] Department of Thoracic Surgery, Shengjing Hospital of China Medical University, Shenyang 110004, China
[b] Department of Anesthesiology, Shengjing Hospital of China Medical University, Shenyang 110004, China
[c] Department of Critical Care Medicine, Shengjing Hospital of China Medical University, Shenyang 110004, China.

ARTICLE INFO

Article history:
Received 10 February 2025
Received in revised form 2 March 2025
Accepted 12 May 2025

Keywords:
Sepsis-induced acute lung injury
Ginsenoside Rb1
AMPK/SIRT1 pathway
Alveolar type II epithelial cells

ABSTRACT

Sepsis-induced acute lung injury (ALI) is a major clinical challenge, with limited treatment options and high mortality. Ginsenoside Rb1, a bioactive compound derived from ginseng, has shown promising anti-inflammatory and antioxidative effects. This study is the first to systematically investigate the metabolites of ginsenoside Rb1, specifically F2 and CK, in the context of sepsis-induced ALI modeled by lipopolysaccharide (LPS) administration, a widely used preclinical approach to mimic key inflammatory features of clinical sepsis. Unlike other studies, which primarily focus on ginsenoside Rb1 itself, our research specifically emphasizes the role of its metabolites in this process. We demonstrated that ginsenoside Rb1 significantly improved lung histopathological damage, reduced inflammation, and inhibited cell apoptosis in a sepsis-induced ALI mouse model. Metabolomics and proteomics analyses revealed that Rb1 is metabolized into F2 and CK, which activate the AMP-activated protein kinase (AMPK)/Sirtuin 1 (SIRT1) signaling pathway. This activation promotes Forkhead Box O1 (FOXO1) deacetylation, inhibiting its cytoplasmic translocation and enhancing mitochondrial unfolded protein response (*mtUPR*) gene transcription. *In vitro* experiments confirmed that ginsenoside Rb1 protected alveolar type II (AT2) cells from oxidative stress and senescence, while restoring mitochondrial function. Blocking the AMPK/SIRT1 pathway or silencing FOXO1 reversed these protective effects, highlighting their crucial roles in Rb1's mitigation of ALI. Our findings provide new insights into the molecular mechanisms by which ginsenoside Rb1 alleviates sepsis-induced ALI and offer a potential therapeutic approach for treating sepsis-related lung injuries.

1. Introduction

Sepsis-induced acute lung injury (ALI) is a lung injury caused by systemic infection, marked by barrier disruption, inflammation, oxidative stress, and apoptosis[1-2]. Sepsis-induced ALI typically accompanies acute respiratory distress syndrome (ARDS), a life-threatening condition with a high mortality rate[3-4]. In this study, we used a lipopolysaccharide (LPS)-induced ALI mouse model, which is widely employed to simulate the acute inflammatory phase of sepsis-induced ALI due to its controllability and reproducibility. While it does not fully replicate the complex pathophysiology of human sepsis, such as immune suppression or polymicrobial infection, it provides a reliable platform to investigate inflammatory signaling pathways in lung injury. Despite various treatment approaches available in clinical practice, such as mechanical ventilation, antibiotics, and fluid management, the prognosis for ALI patients remains suboptimal with persistently high mortality rates[5-7]. Therefore, the search for new therapeutic strategies, particularly interventions based on natural

[1] These authors are regarded as co-first authors.
[*] Corresponding authors.
E-mail address: 20052131@cmu.edu.cn (Z.L. Fu); llgao@cmu.edu.cn (L.L. Gao)
Peer review under responsibility of Beijing Academy of Food Sciences.

SciOpen Publishing services by Tsinghua University Press

http://doi.org/10.26599/FSHW.2025.9250658

products, has become a top priority[7-9]. In recent years, more studies have focused on the potential roles of traditional Chinese medicine and natural products in treating ALI[8,10-11]. Ginsenoside Rb1 has garnered significant attention due to its diverse biological activities[12].

Ginsenoside Rb1 is a triterpene compound extracted from ginseng, exhibiting broad pharmacological effects[13-15]. Studies have indicated that ginsenoside Rb1 displays remarkable effects in inflammation, oxidation, anti-tumor activities, cardiovascular protection, and neuroprotection[16]. In cardiovascular diseases, ginsenoside Rb1 mitigates myocardial damage by inhibiting oxidative stress and inflammatory responses, while in neurological disorders, Rb1 acts as a neuroprotectant by modulating neurotransmitters and reducing neuroinflammation[17-18]. However, the mechanisms underlying the action of ginsenoside Rb1 in sepsis-induced ALI remain unclear. Initial studies suggest that Rb1 may exert a protective effect on lung damage by regulating metabolic pathways and protein expression, but further investigations are needed to elucidate the specific mechanisms[19-20]. This study aims to delve deeper into the mechanisms of action of ginsenoside Rb1 in sepsis-induced ALI, uncovering its potential therapeutic effects.

AMP-activated protein kinase (AMPK) and Sirtuin 1 (SIRT1) are crucial regulatory molecules in cellular energy metabolism and stress responses[21-22]. AMPK, as an intracellular energy sensor, can detect cellular energy status and regulate metabolic pathways to maintain cellular energy balance[23-25]. SIRT1 is a NAD^+-dependent deacetylase that modulates cellular stress responses and metabolism by deacetylating multiple target proteins[26-28]. AMPK can influence various physiological processes downstream, including cell apoptosis, oxidative stress, and mitochondrial function, by directly activating or indirectly regulating SIRT1[29-31]. Studies have shown that the AMPK/SIRT1 signaling pathway is protective in various pathological conditions such as myocardial ischemia, neurodegenerative diseases, and metabolic syndrome[32-33]. Therefore, exploring whether ginsenoside Rb1 exerts its protective effects in sepsis-induced ALI by activating the AMPK/SIRT1 signaling pathway is of significant importance for elucidating its molecular mechanism[34-35].

To systematically elucidate the mechanism of action of ginsenoside Rb1 in sepsis-induced ALI, this study employed stable isotope tracing targeted metabolomics and proteomics techniques in conjunction with an analysis using the sepsis-induced ALI mouse model. The specific methodology included establishing the sepsis-induced ALI mouse model, collecting mouse lung tissues for protein and RNA transcriptome sequencing analysis, labeling Rb1 with ^{13}C isotopes, treating ALI model mice with labeled Rb1, and analyzing metabolites in lung tissues. Additionally, assessments were conducted using hematoxylin and eosin (H&E) staining, the wet-to-dry weight ratio of the lungs, Evan's Blue staining, and TUNEL staining to examine pathological changes in lung tissues, epithelial barrier permeability, and cell apoptosis rate. Oxidative stress-related indicators and cellular and tissue mitochondrial morphology were evaluated through immunofluorescence and biochemical assay kits, while gene expression levels were assessed using reverse transcription quantitative polymerase chain reaction (RT-qPCR). Primary alveolar type II epithelial cells (AT2) were isolated and purified, identified *via* flow cytometry, and used to establish an ALI cell model. Senescence-associated β-galactosidase (SA-β-gal) staining was employed to assess the aging status of various AT2 groups, dual luciferase experiments to investigate the impact of Forkhead Box O1 (FOXO1) on gene promoter transcriptional activity, and chromatin immunoprecipitation (ChIP) experiments to examine the enrichment of FOXO1 on gene promoters. Western blot analysis was utilized to detect protein expression levels, FOXO1 acetylation and phosphorylation, immunofluorescence for FOXO1 nuclear-cytoplasmic localization, and JC-1 staining to measure cellular mitochondrial membrane potential (MMP).

The main aim of this study is to elucidate the molecular mechanism of ginsenoside Rb1 in sepsis-induced ALI, clarifying its role in preventing AT2 aging and alleviating sepsis-induced ALI by activating the AMPK/SIRT1 signaling pathway to promote FOXO1 deacetylation, subsequently activating the transcription of mitochondrial unfolded protein response (mtUPR)-related genes. The research findings contribute to a deeper understanding of the pathogenesis of sepsis-induced ALI and provide a scientific basis for ginsenoside Rb1 as a potential therapeutic agent. Clinically, a clear understanding of the mechanism of action of Rb1 can offer new treatment strategies for ALI patients, improving prognosis and enhancing survival rates. Furthermore, this study may offer new insights and methods for treating other acute and chronic lung diseases, demonstrating significant scientific research and clinical application value.

2. Materials and methods

2.1 Construction of lentiviral vectors

Lentiviral interference vector pSIH1-H1-copGFP (shRNA, catalog number: SI501A-1, System Biosciences, USA) and lentiviral overexpression vector pCDH-CMV-MCS-EF1α-copGFP (oe-, overexpression vector, catalog number: CD511B-1, System Biosciences, USA) were purchased to establish lentivirus-based *SIRT1* gene overexpression vector and *FOXO1* gene interference vector.

The lentivirus particles carrying the vectors were packaged into HEK-293T cells (catalog number: iCell-h237, Cytiva, Shanghai, China) using the lentivirus packaging kit (A35684CN, Invitrogen, USA). The cell culture supernatant collected after 48 h contained the lentivirus, with a titer of 1×10^8 transducing units (TU)/mL. The sequences used were as follows (5′ to 3′): sh-NC sequence: ATTGCAGAACCGTAAGCATTAC; sh-FOXO1-1 sequence: CGGAGGATTGAACCAGTATAA; sh-FOXO1-2 sequence: CCGCCAAACACCAGTCTAAAT.

2.2 Construction of the murine model of sepsis-induced ALI

Male C57BL/6 mice (weight 22–25 g, 8 weeks old) were obtained from Beijing Vital River Laboratory Animal Technology Co., Ltd. (catalog number: 213) and housed in an SPF-grade animal facility with a humidity range of 60%–65% and a temperature range of 22–25 °C. After 1 week of acclimation, the mice were observed for their health status before the experiment commenced. The Institutional Animal Care and Use Committee approved the experimental procedures and animal handling protocols.

Initially, male C57BL/6 mice were randomly assigned to the Control and ALI groups. The method used was as follows: the animals were first stratified based on body weight into several blocks, ensuring that animals within each block had similar body weights. Each animal within a block was then assigned a number, and a random number table was used to randomly allocate the animals into different experimental and control groups. The method for constructing the ALI model involved intratracheal injection of phenol-

extracted and purified LPS (10 mg/kg, catalog number: 916374, Sigma-Aldrich) dissolved in 50 μL of sterile saline[36]. The Control group received an equivalent volume of sterile saline *via* the same route. Lung tissue samples were collected within 12 h post-injection. The lung tissues were frozen in liquid nitrogen and stored at −80 ℃ for further biochemical analysis. Additionally, a portion of the lung tissue was fixed in a 10% formalin solution for subsequent histological analyses.

The ALI model was divided into the following groups, each comprising 6 mice: ALI + Rb1 group (following LPS administration, mice received ginsenoside Rb1 (20 mg/kg) *via* tail vein injection). ALI + F2 group (following LPS administration, mice received ginsenoside F2 (20 mg/kg) *via* tail vein injection). ALI + Compound K (CK) group (following LPS administration, mice received ginsenoside CK (20 mg/kg) *via* tail vein injection). DMSO group (following LPS administration, mice received an equal volume of DMSO *via* tail vein injection (as vehicle control)). Rb1 + DMSO group (following LPS administration, mice were co-treated with Rb1 (20 mg/kg) and DMSO *via* tail vein injection). Rb1 + Compound C group (following LPS administration, mice were co-treated with Rb1 (20 mg/kg) and Compound C (10 mg/kg), an AMPK/SIRT1 pathway inhibitor, *via* tail vein injection). DMSO + sh-NC group (1 week before LPS challenge, mice received sh-NC lentivirus (1 mL/kg) *via* tail vein, followed by DMSO treatment after LPS induction). Rb1 + sh-NC group (1 week before LPS challenge, mice received sh-NC lentivirus (1 mL/kg) *via* tail vein, followed by Rb1 (20 mg/kg) treatment after LPS induction). Rb1 + sh-FOXO1 group (1 week before LPS challenge, mice received sh-FOXO1 lentivirus (1 mL/kg) *via* tail vein, followed by Rb1 (20 mg/kg) treatment after LPS induction). Treatment with ginsenoside Rb1, CK (catalog numbers: 00170580, SMB00348, Sigma-Aldrich), and F2 (catalog number: 62025-49-4, Shanghai BiotechSource) involved intravenous administration of Rb1 at a dose of 20 mg/kg after LPS injection[37]. Compound C, an AMPK/SIRT1 pathway inhibitor (catalog number: HY-13418G, MedChemExpress), was administered at 10 mg/kg *via* the tail vein post-LPS injection. The lentivirus treatment involved a tail vein injection of 1 mL/kg of lentivirus 1 week before LPS injection[38].

2.3 H&E staining

The lung tissue sections of mice were deparaffinized in water after being sliced and mounted on slides. H&E staining was performed following the instructions from the H&E staining kit (PT001, purchased from Shanghai Bogu Biotechnology Co., Ltd., Shanghai, China). The main steps of the staining procedure were as follows: staining with hematoxylin at room temperature for 10 min, rinsing in running water for 30–60 s; differentiation in 1% hydrochloric acid alcohol for 30 s, followed by rinsing and soaking in water for 5 min; eosin staining at room temperature for 1 min; dehydration in a series of alcohol gradients (concentrations of 70%, 80%, 90%, 95%, 100%), with each gradient dehydration step lasting 1 min; clearing with xylene and then 2 rounds of xylene I and II for 1 min each; mounting slides with neutral resin in a fume hood, and finally, examining the morphological changes in lung tissues of each group under an optical microscope (BX50; Olympus Corp., Tokyo, Japan) for photomicrography.

2.4 Wet/dry weight calculation

The water on the surface of the mouse lungs was carefully removed using a clean cotton cloth, and the lung weight (wet weight, *W*) was measured. Subsequently, the tissues were placed in a constant temperature oven at 75 ℃ for 48 h to obtain the dry weight (*D*), from which the lung water content index was calculated as *W*/*D*.

2.5 Evan's blue staining

Evan's Blue dye (catalog number: E2129, Sigma-Aldrich) was used to assess the permeability of the pulmonary epithelial barrier in mouse lung tissues. The procedure involved the following steps: after LPS stimulation, mice were intravenously injected with 2% Evan's Blue dye (2 mL/kg) *via* the tail vein. A total of 5 min later, the abdominal aorta of the mice was cut to allow blood drainage. Subsequently, a cannula was swiftly inserted into the right ventricle through the carotid artery into the pulmonary artery, and 10 mL of cold saline was continuously infused through the cannula to wash out the blood and isolate the entire lung from circulation. The lung tissue was then immediately weighed, homogenized with 1 mL of trichloroacetic acid solution (50%), and centrifuged at 13 000 r/min for 0.5 h. The supernatant was diluted with ethanol (1:3), and its absorbance was measured at 630 nm using a microplate reader.

2.6 TUNEL staining

The TUNEL Apoptosis Detection Kit-DAB (catalog number: abs50022, obtained from Abbkine Scientific Co., Ltd., Shanghai, China) was utilized to assess cell apoptosis in lung tissue. The procedure involved incubating lung tissue slices at room temperature in the terminal deoxynucleotidyl transferase (TdT)/nucleotide complex for 1 h, followed by PBS washing and nuclear labeling with horseradish peroxidase and diaminobenzidine. Subsequently, counterstaining was performed with hematoxylin. Apoptotic cells were observed under an optical microscope, and images were captured (cells stained brown indicated positive staining). A total of 5 random fields were selected on each slide for cell apoptosis detection. The apoptotic rate was expressed as the percentage of positive cells, calculated as the number of apoptotic positive cells divided by the total cell count, multiplied by 100%.

2.7 Oxidative stress assessment

The levels of reactive oxygen species (ROS) in lung tissue and cells were determined using CellROX^{TM} Deep Red (catalog number: C10443, ThermoFisher, USA) and DCFH-DA (catalog number: C2938, ThermoFisher, USA) staining methods. Mitochondrial ROS was measured based on the fluorescence results of MitoSOX live-cell imaging. Lung tissue and cell fluorescence staining were observed *via* confocal microscopy (Leica TCS SP5, Wetzlar, Germany), with the average intensity of the fluorescence calculated using ImageJ software.

The total superoxide dismutase (SOD) activity was determined through the WST-1 assay (catalog number: BC5165, Solable Biological Technology Co., Ltd., Beijing, China), while the activity of thiobarbituric acid reactive substances (TBARS) was measured using a colorimetric method.

2.8 RT-qPCR

Total RNA was extracted from tissues and cells using TRIzol (ThermoFisher, USA) and assessed for concentration and purity using the nanodrop 2000 UV-vis spectrophotometer (ThermoFisher, USA). mRNA was reverse transcribed into cDNA following the instructions of the PrimeScript RT reagent kit (Takara, Japan). Primers for each gene were synthesized by TaKaRa (Table S1). RT-qPCR was performed on a 7500 Fast system (ThermoFisher, USA) using *GAPDH* as the reference gene. The relative transcription levels of the target genes were calculated using the comparative method ($2^{-\Delta\Delta Ct}$ method) as ΔΔCt = ΔCt experimental group − ΔCt control group, where ΔCt = Ct (target gene) − Ct (reference gene), and the relative mRNA transcription level of the target gene was determined as $2^{-\Delta\Delta Ct}$. Each experiment was performed in triplicate.

2.9 Isolation and identification of primary AT2 cells in mice

AT2 cells were isolated and purified from mice using membrane filtration and immunoadhesion methods. Specifically, lung tissues were taken from mice after disinfection with 75% ethanol, digested with trypsin and collagenase, and red blood cells were removed using a lysis buffer. The cell suspension was then preliminarily filtered to separate AT2 cells based on size. Since AT1 cells and macrophages are larger than AT2 cells, a preliminary filtration using a 74 μm filter membrane was carried out to eliminate large tissue fragments. Subsequently, a second filtration using a 38 μm filter membrane was performed to thoroughly remove all AT1 cells and some remaining macrophages. Lastly, AT2 cells were filtered through a 19 μm filter membrane and purified through immunoadhesion using plastic plates coated with immunoglobulin G (IgG). The AT2 cells were cultured for 72 h in a 37 ℃, 5% CO_2 environment with 10% fetal bovine serum (FBS) and Ham's F-12K medium (Catalog number: 21127022, ThermoFisher, USA). Identification of AT2 cells was conducted using flow cytometry with surfactant protein C (SP-C) positivity as the standard.

2.10 Cell grouping and treatment

To establish an ALP cell model, AT2 cells were stimulated with LPS (100 μg/mL) for 6 h, with an equal volume of PBS as the control group. AT2 cells in the LPS group were further divided into several groups as follows: LPS + Rb1 group (cells stimulated with LPS and treated with ginsenoside Rb1 (20 μmol/L)). sh-NC group (cells stimulated with LPS and transfected with negative control short hairpin RNA (sh-NC)). sh-FOXO1 group (cells stimulated with LPS and transfected with FOXO1-targeting shRNA). oe-NC group (cells stimulated with LPS and transfected with empty vector for overexpression control). or-SIRT1 group (cells stimulated with LPS and transfected to overexpress SIRT1). DMSO group (cells stimulated with LPS and treated with an equal volume of dimethyl sulfoxide (DMSO), serving as the solvent control for Compound C). Rb1 + DMSO group (cells stimulated with LPS and co-treated with ginsenoside Rb1 (20 μmol/L) and DMSO). Rb1 + Compound C group (cells stimulated with LPS and co-treated with ginsenoside Rb1 (20 μmol/L) and Compound C (10 μmol/L), an AMPK/SIRT1 pathway inhibitor). DMSO + sh-NC group (cells stimulated with LPS and treated with DMSO and sh-NC lentivirus). Rb1 + sh-NC group (cells stimulated with LPS and co-treated with ginsenoside Rb1 (20 μmol/L) and sh-NC lentivirus). Rb1 + sh-FOXO1 group (cells stimulated with LPS and co-treated with ginsenoside Rb1 (20 μmol/L) and FOXO1-targeting shRNA lentivirus). In these groups, Rb1 treatment involved adding 20 μmol/L of Rb1 to the cells, Compound C treatment involved adding 10 μmol/L of Compound C to the cells, and lentivirus treatment involved introducing 1 mL of the corresponding lentivirus into the cells, with lentiviral infection efficacy assessed 48 h post-treatment.

2.11 Cell senescence assay using SA-β-gal staining

Cells in a 6-well plate were aspirated, washed once with PBS, and then 1 mL of SA-β-gal staining fixative solution (catalog number: K146501, ThermoFisher, USA) was added to each well. The cells were fixed at room temperature for 20 min, the staining fixative solution was aspirated, and the cells were washed three times with PBS for 3 min each. After removing the PBS, 1 mL of staining working solution was added to each well. The plate was sealed with a cover membrane to prevent evaporation and then incubated overnight at 37 ℃. Cell counting and observation were conducted under a light microscope. This experimental procedure was repeated 3 times.

2.12 Analysis of metabolites of ginsenoside Rb1

To analyze the metabolites of ginsenoside Rb1, we employed ^{13}C isotope labeling and treated ALI model mice with labeled Rb1. Following treatment, lung tissues from the mice were collected for metabolite analysis. The labeled metabolites were initially analyzed using nuclear magnetic resonance (NMR). Lung tissue samples were extracted and processed to ensure the purity and concentration of metabolites were suitable for NMR analysis. The NMR analysis was conducted on a 600 MHz NMR spectrometer, with ^{13}C-NMR spectra used to detect the ^{13}C isotope-labeled metabolites.

Subsequently, we employed matrix-assisted laser desorption/ionization time-of-flight mass spectrometry (MALDI-TOF-MS) to further characterize the structure of the metabolites. Following appropriate sample preparation, lung tissue samples were coated onto a MALDI target plate and mixed with a matrix. Mass spectrometry analysis was then carried out on the MALDI-TOF-MS instrument, where ion modes in the sample were detected and analyzed using TOF-MS to confirm and characterize the structure of the metabolites of ginsenoside Rb1.

2.13 Proteomic and transcriptomic sequencing

In order to comprehensively understand the protein expression and gene transcription in lung tissues under different treatment conditions, we conducted proteomic and transcriptomic sequencing analyses. Initially, lung tissue samples from treated mice were rapidly frozen and stored at –80 ℃ to ensure sample quality. Proteomic analysis utilized mass spectrometry technology. The lung tissue samples were lysed and proteins extracted, followed by protein digestion with trypsin and liquid chromatography-tandem mass spectrometry (LC-MS/MS) analysis. Mass spectrometry data were subjected to database searches for protein identification and quantitative analysis to determine differences in protein expression under different treatment conditions.

Regarding transcriptomic sequencing (RNA-seq) analysis, total RNA was extracted from lung tissues using an RNA extraction kit to ensure RNA integrity and purity. mRNA was enriched through methods such as poly-A enrichment or ribosomal RNA depletion. Subsequently, libraries were constructed and subjected to paired-end sequencing using high-throughput sequencing platforms like Illumina HiSeq. The raw sequencing data underwent quality control filtering, alignment, and annotation, followed by analysis of gene expression levels using standard bioinformatics software. Differentially expressed gene (DEG) analysis identified genes significantly altered under different treatment conditions.

2.14 Bioinformatics analysis

The "limma" package in R was utilized to analyze proteomic and transcriptomic sequencing data, with a criterion of P-value < 0.05 and $|\log_2 FC| > 1$ set as the threshold for selecting significant DEGs. Subsequently, the "ClusterProfiler" package in R was employed for Gene Ontology (GO) and Kyoto Encyclopedia of Genes and Genomes (KEGG) enrichment analysis of DEGs, and the results were visualized using the "ggplot2" package. A protein-protein interaction (PPI) network was constructed based on the top 20 significantly upregulated proteins to identify core proteins, downstream target genes of FOXO1 were predicted on the JASPAR website, and an intersection was taken with mtUPR-related genes.

2.15 Detection of FOXO1 protein acetylation

To assess the acetylation status of intracellular FOXO1 protein, an immunoprecipitation (IP) method was employed. Initially, cells were lysed, and cell debris was removed by centrifugation to obtain the supernatant. Protein A/G magnetic beads (catalog number: 88803, ThermoFisher, USA) were utilized to pre-clearance the lysates and reduce nonspecific binding. Subsequently, an anti-FOXO1 antibody (1:50, #2880, CST, USA) was added to the supernatant and incubated overnight at 4 ℃ to form a complex of the antibody with the target protein. The complex was then captured by protein A/G magnetic beads, subjected to multiple washes, treated with SDS loading buffer to release the proteins, and separated by SDS-PAGE. Finally, acetylated FOXO1 was detected using a Western blot technique with an anti-acetyl-lysine antibody (1:1 000, #9441, CST, USA) to evaluate its acetylation level.

2.16 Western blot analysis

Total proteins from tissues or cells were extracted using RIPA lysis buffer containing PMSF (P0013C, Beyotime, Shanghai, China). The extraction process involved a 30-min incubation on ice followed by centrifugation at 8 000 × g at 4 ℃ for 10 min to collect the supernatant. The concentration of total proteins was determined using a BCA assay kit (catalog number: 23227, ThermoFisher, USA). Subsequently, 50 μg of proteins were dissolved in 2× SDS sample buffer, boiled at 100 ℃ for 5 min, loaded onto SDS-PAGE gels for electrophoresis, and transferred onto PVDF membranes. The membranes were then blocked with 5% non-fat milk at room temperature for 1 h and subsequently probed with primary antibodies against SIRT1 (1:1 000, ab189494, Abcam, Cambridge, UK), AMPK (1:1 500, ab32047, Abcam, Cambridge, UK), p-AMPK (1:1 000, ab133448, Abcam, Cambridge, UK), p-FOXO1 (1:2 000, ab259337, Abcam, Cambridge, UK), FOXO1 (1:1 000, #2880, CST, USA), acetylated-lysine (1:1 000, #9441, CST, USA), and GAPDH (ab9485, 1:2 500, Abcam, Cambridge, UK) as the loading control. The membranes were then incubated overnight at 4 ℃, washed 3 times with TBST for 10 min each, and incubated with an HRP-conjugated secondary antibody (goat anti-rabbit IgG H&L HRP, ab97051, 1:2 000, Abcam, Cambridge, UK) for 1 h. After washing with TBST, the membranes were placed on a clean glass plate. ECL fluorescence detection reagents from abs920 (Elabscience, Shanghai, China) were mixed in equal proportions, applied onto the membranes, and visualized using a Bio-Rad imaging system (Bio-Rad, USA). Image analysis was performed using Quantity One v4.6.2 software to determine the relative protein levels represented as the grayscale intensity ratio of the corresponding protein bands to the GAPDH protein band. The experiment was repeated 3 times, and the average values were calculated.

2.17 Cell immunofluorescence

Cells were cultured in immunofluorescence chambers with 2×10^5 cells/well. When the cell confluency reached about 90%, cells were washed thrice with PBS. Fixation was done by adding 1 mL of 4% paraformaldehyde per well and incubating at room temperature for 15 min. After 3 washes with PBS, cells were permeabilized with 0.3% Triton for 10 min, followed by another 3 PBS washes. Subsequently, cells were blocked with goat serum (catalog number: 16210072, ThermoFisher, USA) for 30 min. Cells were washed three times with PBS, and incubated with primary anti-FOXO1 antibody (1:50, #2880, CST, USA) diluted in PBS overnight at 4 ℃. After 3 PBS washes, cells were treated with secondary antibody goat anti-rabbit IgG H&L (Alexa Fluor 647) (1:200, ab150079, Abcam, Cambridge, UK) at room temperature in the dark for 1 h. Following 3 PBS washes, cells were stained with DAPI for 15 min, washed 3 times with PBS in the dark, and mounted with a fluorescence quenching agent (catalog number: P36961, ThermoFisher, USA). The samples were then observed and photographed under a fluorescence microscope, and ImageJ software was utilized to analyze fluorescence intensity.

2.18 Dual-luciferase assay

sh-NC and sh-FOXO1 were co-transfected with dual-luciferase reporter gene vectors containing Lon peptidase 1, mitochondrial (LONP1), SOD2, heat shock protein family D member 1 (HSPD1), heat shock protein family e member 1 (HSPE1), and catalase (CAT) promoter sequences, along with their corresponding mutant binding sites. This co-transfection was carried out in human embryonic kidney HEK293T cells using Lipofectamine 2000 reagent (catalog number: 11668019, ThermoFisher, USA) to investigate the impact of FOXO1 on the transcriptional activity of LONP1, SOD2, HSPD1, HSPE1, and CAT promoters. Renilla luciferase was used as the internal control. After 48 h post-transfection, cells were harvested, lysed, and subjected to luciferase assay using the luciferase assay kit (K801-200, Biovision, USA). The firefly luciferase activity was measured with the Dual-Luciferase Reporter Gene Analysis System (Promega, Madison, WI, USA). The target reporter gene activation

level was normalized by calculating the firefly luciferase-determined value RLU ratio to the Renilla luciferase-determined value RLU.

2.19 ChIP experiment

A ChIP assay kit (catalog number: KT101-02, Saicheng Biotech Co., Ltd., Guangzhou, China) was employed to investigate the enrichment of FOXO1 within the promoter regions of *LONP1*, *SOD2*, *HSPD1*, *HSPE1*, and *CAT* genes. The procedure involved the following steps: once the cell confluency reached 70%–80%, 1% formaldehyde was added to crosslink the DNA and proteins within the cells at room temperature for 10 min. Subsequently, the cross-linked chromatin was sonicated to shear into suitable-sized fragments by sonicating for 10 s, pausing for 10 s, and repeating this cycle 15 times. After centrifugation at 13 000 r/min at 4 ℃, the supernatant was collected and divided into 2 tubes. One tube was incubated with a negative control antibody, rabbit anti-IgG (ab172730, 1:100, Abcam, UK), and the other with a specific antibody against the target protein, rabbit anti-FOXO1 (1:50, #2880, CST, USA). Following overnight incubation at 4 ℃, the intrinsic DNA-protein complexes were precipitated using Protein Agarose/Sepharose, the supernatant was discarded after brief centrifugation, nonspecific complexes were washed, and the cross-linking was reversed overnight at 65 ℃. The DNA fragments were then purified by phenol/chloroform extraction, and the recovered DNA fragments were used for qPCR to detect the promoter regions of *LONP1*, *SOD2*, *HSPD1*, *HSPE1*, and *CAT* genes (Table S2).

2.20 Measurement of autophagic flux

Cells were transfected with Ad-mRFP-GFP-LC3 (Beyotime Biotechnology, Shanghai, China) to assess autophagic flux for 24 h. The strong red fluorescence of the LC3 protein indicates the presence of autolysosomes formed in the acidic lysosomal environment, reflecting efficient mitochondrial autophagic flux. Conversely, strong green fluorescence of LC3 protein suggests that autophagosomes have not matured into autolysosomes, indicating autophagic flux blockade. The numbers of red and green punctate structures were quantified using the image analysis software ImageJ software.

2.21 Cell and tissue mitochondrial morphology

Mitochondria in cells were labeled with MitoTracker Deep Red (100 nmol/L) for 30 min at 37 ℃ and visualized using confocal microscopy (Leica TCS SP5, Wetzlar, Germany). Mitochondrial fluorescence clusters were excited with a 633 nm laser and recorded at 558–617 nm for emission. The length of mitochondria was determined and calculated using ImageJ software. Fixed specimens were imaged using an H-7500 transmission electron microscope (Hitachi, Japan) for lung tissue samples. ImageJ software calculates the mitochondrial length and cristae density in the tissue.

2.22 Detection of MMP

Cell samples were washed with culture medium, re-suspended, and prepared on glass slides. JC-1 dye (Catalog number: T3168, ThermoFisher, USA) was used for staining following the manufacturer's instructions. The observation was performed under a fluorescence microscope with an excitation wavelength of 488 nm and an emission wavelength of 590 nm to generate red/green fluorescence. JC-1 forms aggregates and emits red fluorescence in a high MMP state. Conversely, in a low MMP state, JC-1 remains in a monomeric form and emits green fluorescence.

2.23 Animal ethics statement

This study strictly adhered to national laws and regulations regarding the use of laboratory animals and obtained approval from the appropriate ethics review committee. All animal experiments were approved by the Animal Ethics Committee of Shengjing Hospital of China Medical University (CMUKT20241855). All experimental animals were sourced from legal and regulated suppliers and housed in conditions compliant with national laws on animal welfare. Throughout the experiments, all necessary measures were taken to minimize the pain and distress of the animals. The experimental design followed the replacement, reduction, and refinement principles, aiming to minimize the number of animals used and optimize experimental conditions to enhance scientific efficiency and reduce the burden on animals. All surgeries were conducted under appropriate anesthesia and analgesia to ensure the animals experienced as little pain as possible during the experiments. Trained technicians or researchers carried out animal care and experimental procedures to maximize the scientific validity of the experiments and animal welfare. After the study, animals were disposed of humanely and scientifically soundly.

2.24 Statistical analysis

The research data was analyzed using SPSS software (version 21.0, IBM, USA). Descriptive statistics for quantitative data were presented as mean ± standard deviation (SD). Two groups with normally distributed data were compared using an unpaired Student's *t*-test, while comparisons among multiple groups were assessed using one-way ANOVA followed by Tukey's post-hoc test.

3. Results

3.1 Ginsenoside Rb1 alleviates sepsis-induced ALI

ALI is a leading cause of high mortality rates, with current treatment options being limited and often ineffective. In recent years, ginsenoside Rb1 has emerged as a research hotspot for potential therapeutic strategies due to its remarkable anti-inflammatory and antioxidant properties[39]. This study aims to investigate the alleviating effects of ginsenoside Rb1 on sepsis-induced ALI and its underlying mechanisms.

We established a sepsis-induced ALI model in mice through LPS treatment and treated them with ginsenoside Rb1. Results revealed that untreated ALI mice exhibited significant pathological lung injuries, such as thickening of alveolar walls, inflammatory cell infiltration, and edema. However, treatment with Rb1 significantly alleviated the extent of lung damage in mice (Fig. 1A) and reduced the lung wet-to-dry weight ratio of ALI mice (Fig. 1B). Evan's Blue staining demonstrated that the pulmonary epithelial barrier permeability in ALI mice was significantly increased, which was notably reduced following Rb1 treatment (Fig. 1C). TUNEL staining

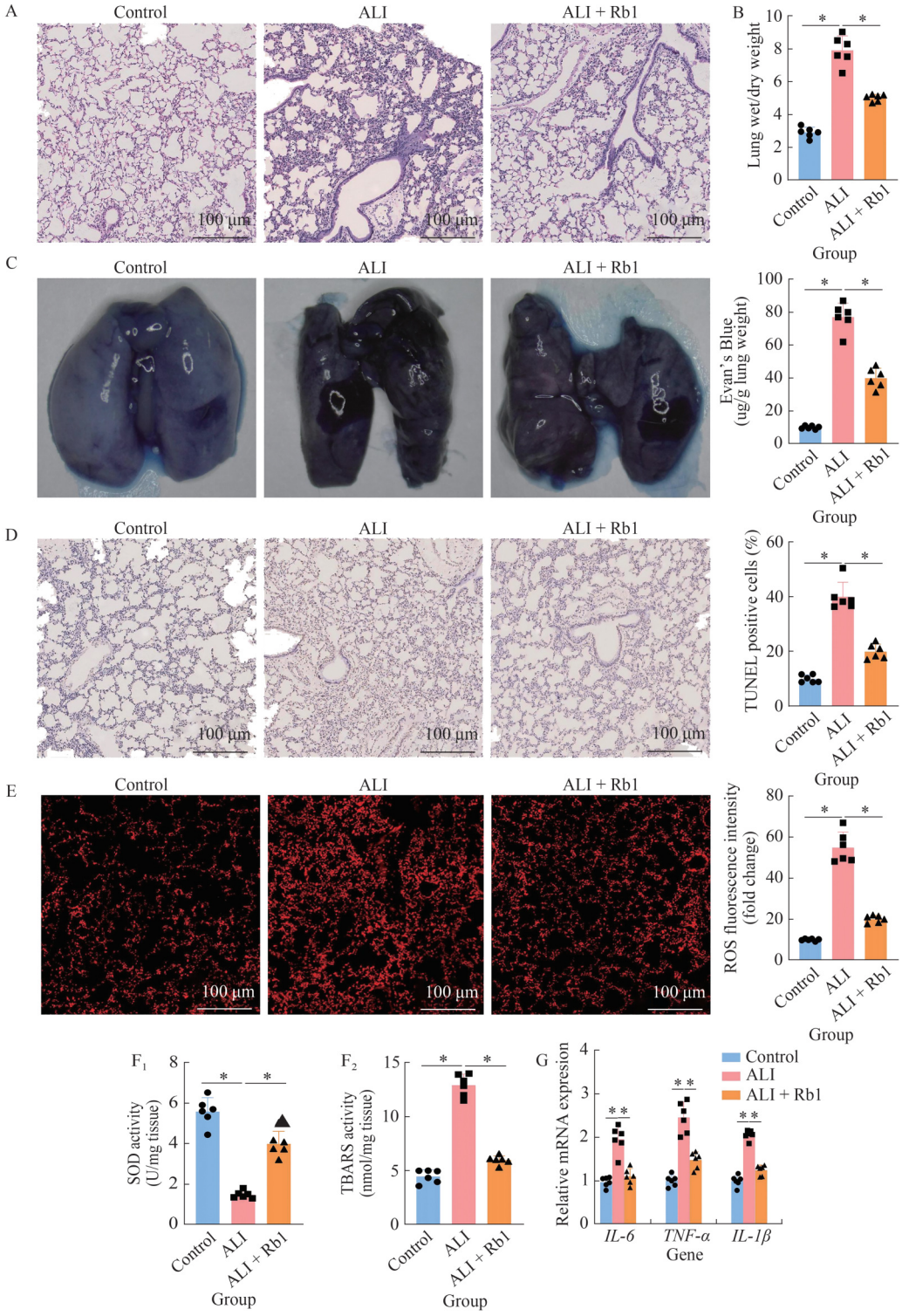

Fig. 1 Effects of ginsenoside Rb1 on sepsis-induced ALI. (A) H&E staining showing pathological changes in lung tissues of different groups of mice. Scale bar = 100 μm; (B) Statistical analysis of the lung wet-to-dry weight ratio in each group of mice; (C) Evan's Blue staining assessing the epithelial barrier permeability of lung tissues in mice; (D) TUNEL staining detecting the apoptosis rate in lung tissues. Scale bar = 100 μm; (E) Fluorescent staining of ROS in lung tissues of each group of mice. Scale bar = 100 μm; (F) Activity levels of oxidative stress markers TBARS and SOD in lung tissues of each group; (G) RT-qPCR analysis of pro-inflammatory cytokine expression levels in lung tissues of each group. *$P < 0.05$ when comparing 2 groups, $n = 6$.

analysis revealed a significant increase in cell apoptosis rates in ALI mice lung tissues, effectively reduced by Rb1 treatment (Fig. 1D). Additionally, in the lung tissues of ALI mice, oxidative stress markers, including ROS levels and TBARS activity, were significantly elevated, while SOD activity was significantly decreased (Figs. 1E and F). Pro-inflammatory genes interleukin-6 (*IL-6*), tumor necrosis factor-alpha (*TNF-α*), and *IL-1β* (Fig. 1G) were markedly higher in the ALI group compared to the control group, and these results were reversed following Rb1 treatment. These findings suggest that Rb1 treatment significantly inhibits the inflammatory response in lung tissues of ALI mice.

Next, we isolated and purified primary AT2 from mice and identified the obtained AT2 cells through flow cytometry based on SP-C positivity (Fig. 2A). *In vitro*, we stimulated AT2 cells with LPS to create an ALP cell model and treated them with ginsenoside Rb1. The study results indicated that LPS stimulation significantly increased the expression of pro-inflammatory genes and ROS levels in AT2 cells while decreasing the activity of the antioxidant enzyme SOD; however, Rb1 treatment effectively reversed these changes (Figs. 2B-E). Known for their junctional function and the inhibition of AT2 senescence in maintaining lung tissue integrity and function[38,40], SA-β-gal staining revealed that Rb1 treatment prevented LPS-induced AT2 senescence (Fig. 2F). Furthermore, Rb1 treatment significantly reduced the expression levels of cell senescence-related markers such as *p16*, *p21*, and the pro-apoptotic gene Bcl-2-associated X protein (*Bax*), while enhancing the expression of cell junction markers zonula occludens-1 (*ZO-1*), *Occludin*, and *Claudin-3* (Figs. 2G and H). These findings suggest that ginsenoside Rb1 can prevent AT2 cell senescence (Fig. 2I).

The above studies demonstrate that ginsenoside Rb1 significantly alleviates sepsis-induced ALI and improves the structure and function of lung tissue at the cellular level.

3.2 Metabolites of ginsenoside Rb1 exhibit anti-inflammatory effects

Investigating the metabolites of ginsenoside Rb1 contributes to a deeper understanding of its anti-inflammatory mechanisms, leading to the development of more effective treatment methods and drugs. We utilized ^{13}C isotope-labeled Rb1 to treat ALI model mice, conducted metabolic analysis on lung tissues, and identified the ^{13}C isotope-labeled metabolites ginsenoside F2 and CK through NMR analysis (Fig. 3A). Subsequently, we further characterized the structures of F2 and CK using MALDI-TOF-MS (Fig. 3B).

These metabolites exhibited a significant increase in concentration in lung tissues (Fig. 3C) and demonstrated notable anti-inflammatory effects by inhibiting the expression of pro-inflammatory genes *IL-6*, *TNF-α*, *IL-1β* (Figs. 3D and E), reducing ROS levels and TBARS activity, and enhancing the activity of the antioxidant enzyme SOD (Figs. 3F and G). These results suggest that the metabolites F2 and CK of ginsenoside Rb1 play a crucial role in the anti-inflammatory effects of ginsenoside Rb1.

3.3 The mechanism of ginsenoside Rb1 alleviating sepsis-induced ALI through the AMPK/SIRT1 signaling pathway

To further elucidate the specific mechanism by which ginsenoside Rb1 alleviates sepsis-induced ALI, we conducted proteomic sequencing analysis on lung tissues from untreated ALI mice and Rb1-treated ALI mice. We identified differentially expressed proteins in lung tissues after Rb1 treatment and selected all upregulated proteins for GO and KEGG enrichment analysis. The results showed that these proteins significantly enriched in functions related to mtUPR, such as "protein folding" "response to oxidative stress" "mitochondrial outer membrane", and "antioxidant activity" (Figs. 4A and B). Additionally, they significantly enriched mitochondrial autophagy, longevity regulation,

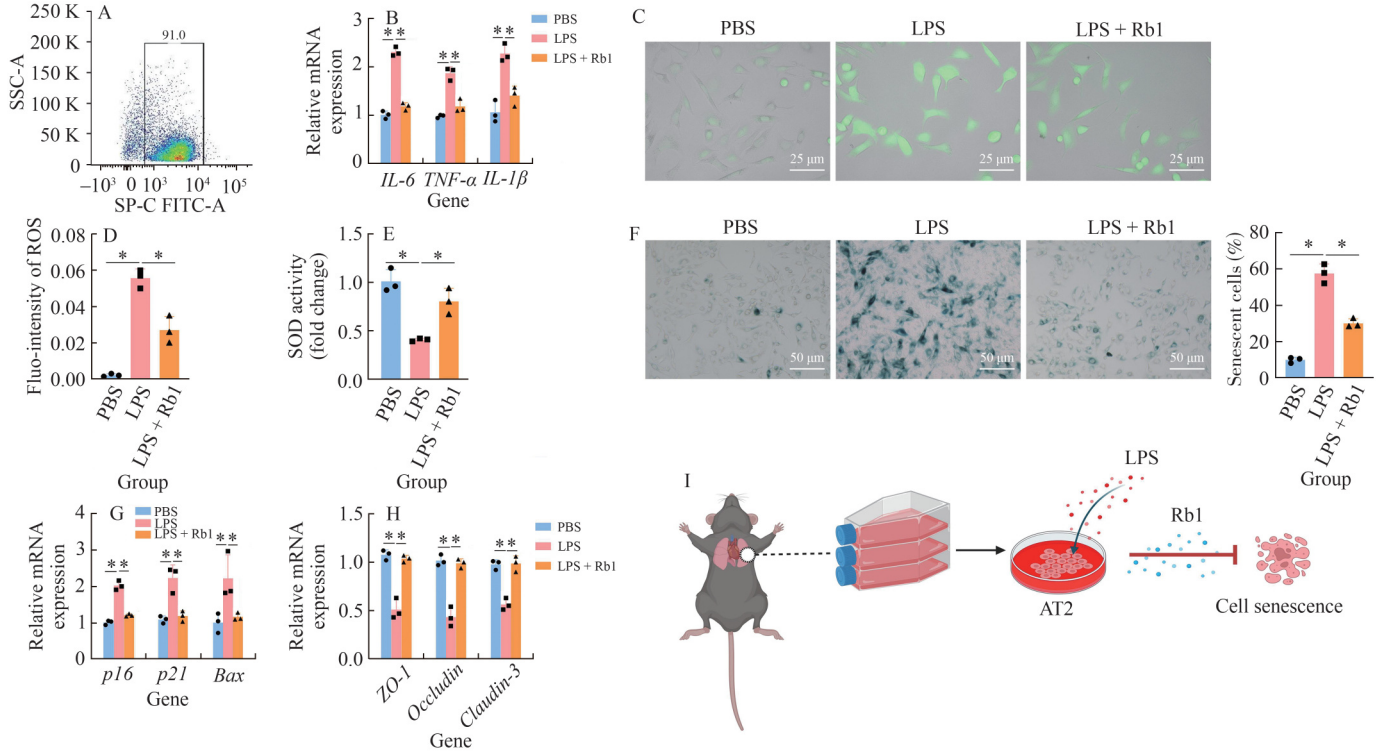

Fig. 2 Effects of ginsenoside Rb1 on AT2 cell senescence. (A) Flow cytometry identification of AT2 cells using SP-C positivity as a marker; (B) RT-qPCR analysis of pro-inflammatory cytokine expression levels in each group of cells; (C-D) DCFH-DA staining to detect ROS production in each group of cells. Scale bar = 20 μm; (E) Activity levels of oxidative stress marker SOD in each group of cells; (F) SA-β-gal staining to assess senescence in each group of AT2 cells. Scale bar = 50 μm; (G) RT-qPCR analysis of senescence-related markers such as *p16*, *p21*, and the pro-apoptotic gene *Bax* in each group of cells; (H) RT-qPCR analysis of cell junction markers *ZO-1*, *Occludin*, and *Claudin-3* in each group of cells; (I) Schematic diagram illustrating how Rb1 prevents AT2 cell senescence. *$P < 0.05$ when comparing 2 groups; all cell experiments were repeated 3 times.

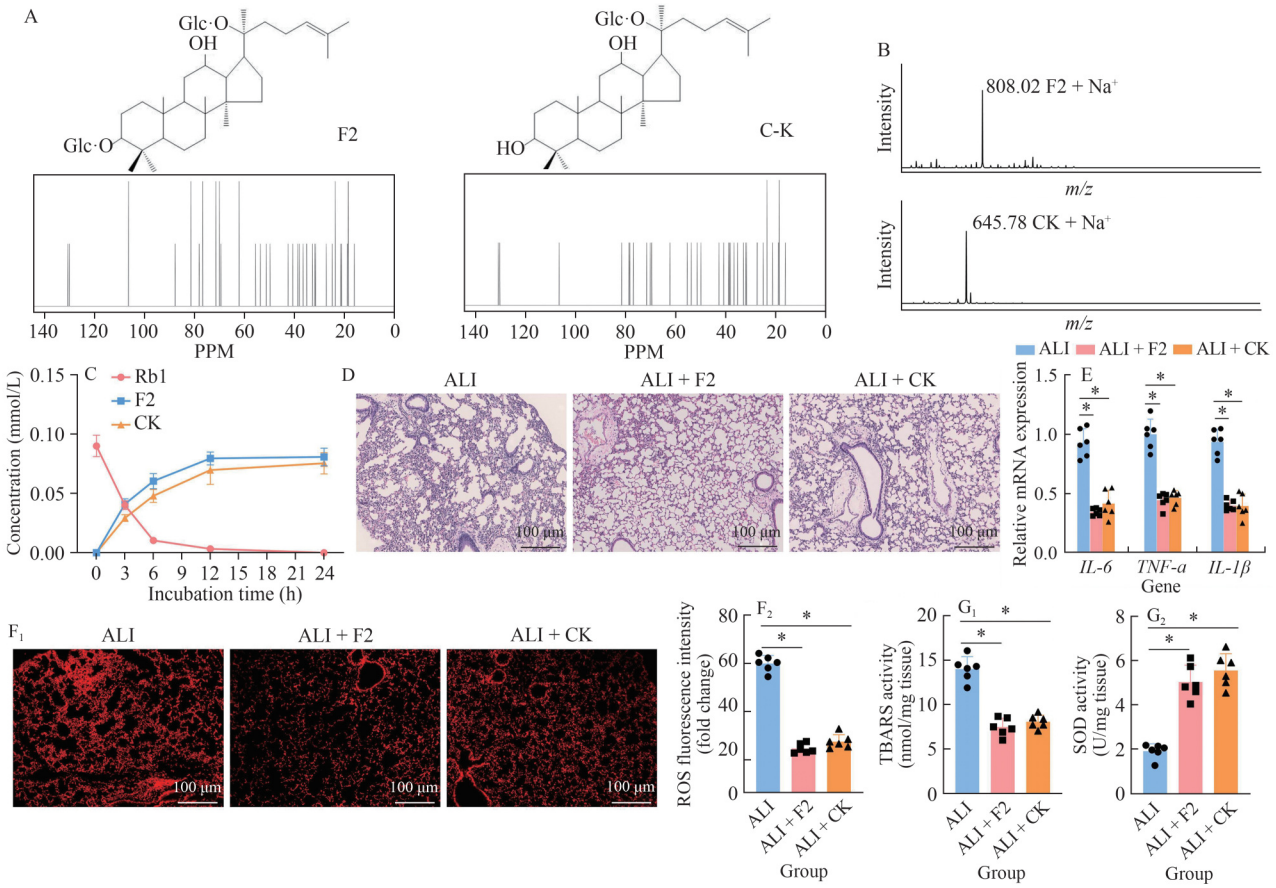

Fig. 3 Analysis of ginsenoside Rb1 metabolites. (A) ^{13}C NMR spectra of ginsenoside Rb1 metabolites F2 and CK; (B) MALDI-TOF-MS analysis of the molecular weight of F2 and CK; (C) Concentration changes of ginsenoside Rb1 and its metabolites F2 and CK in lung tissues; (D) H&E staining showing pathological changes in lung tissues of different groups of mice. Scale bar = 100 μm; (E) RT-qPCR analysis of pro-inflammatory cytokine expression levels in lung tissues of each group of mice; (F) Fluorescent staining of ROS in each group. Scale bar = 100 μm; (G) Activity levels of oxidative stress markers TBARS and SOD in lung tissues of each group. *$P < 0.05$ when comparing 2 groups, $n = 6$.

and energy metabolism AMPK signaling pathways (Figs. 4C and D). Previous studies have confirmed that mtUPR is primarily involved in repairing mitochondrial damage, and there is a close interaction between the AMPK/SIRT1 pathway and mtUPR, playing important roles in maintaining mitochondrial function and cellular homeostasis[41]. Therefore, we hypothesize that ginsenoside Rb1 may participate in repairing ALI by regulating the AMPK/SIRT1 signaling pathway.

Next, we treated AT2 cells with Rb1 and its metabolites F2 and CK and performed Western blot analysis to detect AMPK/SIRT1 signaling pathway-related proteins. Compared to the PBS group, the phosphorylation level of AMPK and the expression of SIRT1 in AT2 cells were significantly decreased in the LPS group. However, after treatment with Rb1, F2, and CK, the phosphorylation level of AMPK and the expression of SIRT1 in AT2 cells were significantly increased

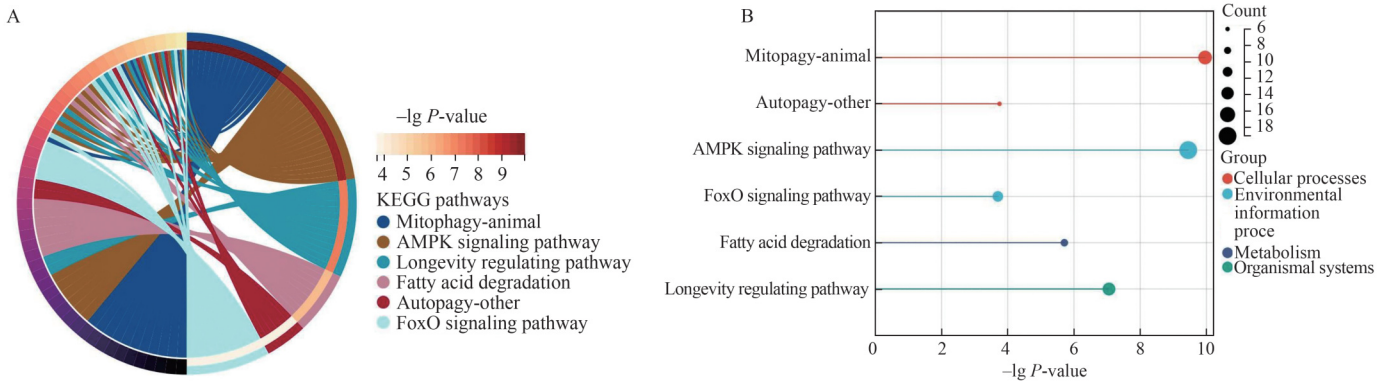

Fig. 4 Impact of ginsenoside Rb1, its metabolites F2, and CK on the AMPK/SIRT1 signaling pathway. (A, B) KEGG enrichment analysis of differentially expressed proteins in lung tissue after Rb1 treatment; (C, D) GO enrichment analysis of differentially expressed proteins in lung tissue after Rb1 treatment; (E) Western blot analysis of AMPK/SIRT1 signaling pathway-related proteins in cells from each group. *$P < 0.05$ when comparing 2 groups. All cellular experiments were replicated 3 times.

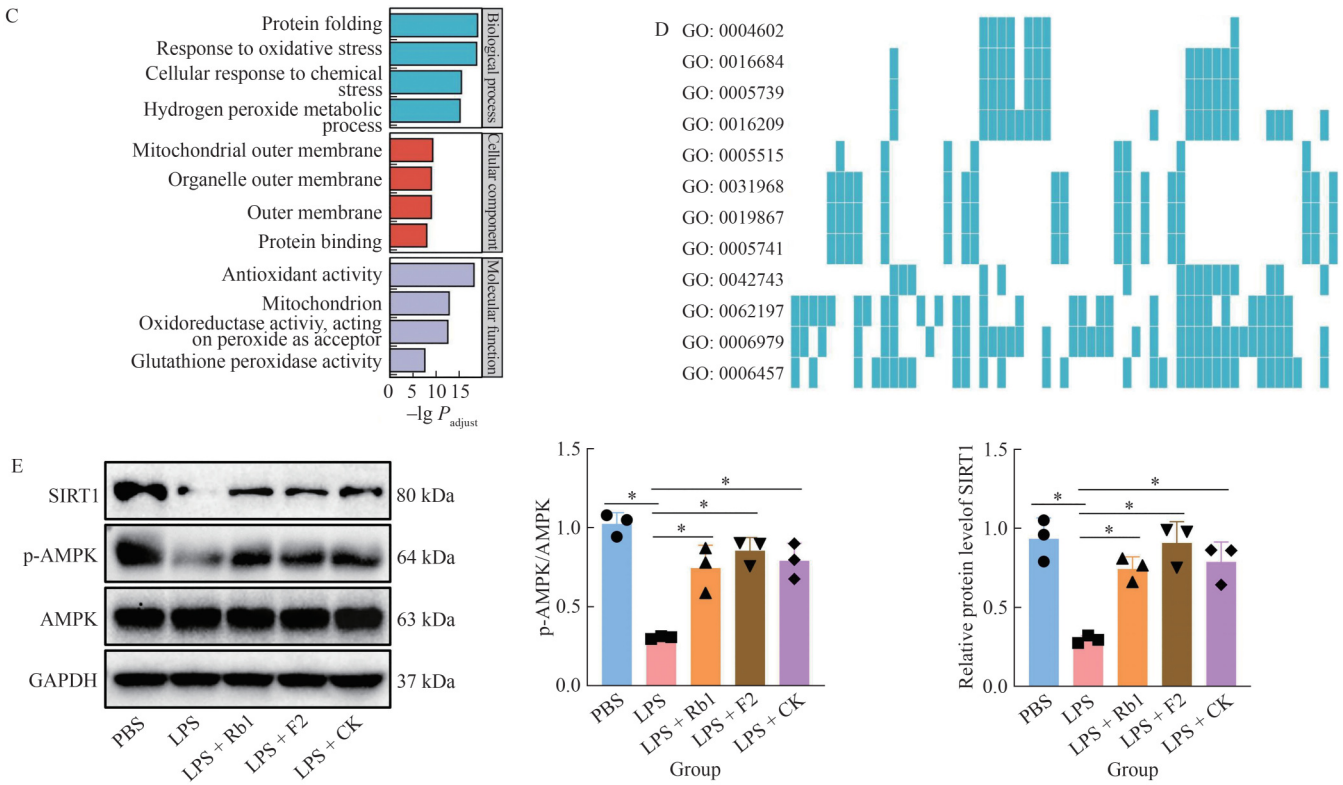

Fig. 4 (*Continued*)

compared to the LPS group (Fig. 4E), indicating that ginsenoside Rb1 and its metabolites F2 and CK can activate the energy metabolism AMPK/SIRT1 signaling pathway.

3.4 Ginsenoside Rb1 activates the AMPK/SIRT1 pathway to promote FOXO1 deacetylation and nuclear translocation, activating the transcription of mtUPR-related genes

Based on the significant upregulation of the top 20 proteins, we constructed a PPI network (Fig. 5A) and identified the transcription factor FOXO1 at a central position (Figs. 5B and C). It is known that mtUPR can transmit signals of mitochondrial damage from mitochondria to the nucleus, triggering the transcription of specific genes. Therefore, we further conducted transcriptomic sequencing analysis of lung tissues from ALI mice, screened DEGs, and performed GO/KEGG enrichment analysis on these genes. The results were similar to those of the differentially expressed proteins, all enriched in mtUPR-related functions and pathways (Figs. S1A-D), indicating that the cellular regulation of mtUPR is consistent at the gene and protein levels under specific conditions. This underscores the critical role of mtUPR in cellular responses.

Subsequently, by intersecting mtUPR-related genes with the top 50 most significantly upregulated genes, we identified 5 differentially expressed mtUPR-related genes: *LONP1*, *SOD2*, *HSPD1*, *HSPE1*, and *CAT* (Figs. 5D and E), and predicted their binding sites with the core protein FOXO1 (Fig. 5F, Table S3). To confirm the transcriptional regulatory relationship between FOXO1 and LONP1, SOD2, HSPD1, HSPE1, and CAT, we first silenced *FOXO1* in AT2 cells. The RT-qPCR results revealed (Fig. S2A) that after silencing *FOXO1*, the expression levels of *FOXO1* in AT2 significantly decreased. The sh-FOXO1-1 had a better silencing effect and was used for subsequent experiments. Upon silencing *FOXO1*, we observed a significant decrease in the expression levels of *LONP1*, *SOD2*, *HSPD1*, *HSPE1*, and *CAT* (Fig. S2B). The dual luciferase assay results showed (Fig. S2C) that after *FOXO1* silencing, the promoter activity of *LONP1*, *SOD2*, *HSPD1*, *HSPE1*, and *CAT* significantly decreased, while their mutant groups showed no significant changes. ChIP experiments (Fig. S2D) indicated a significant reduction in *FOXO1* enrichment on the promoters of *LONP1*, *SOD2*, *HSPD1*, HSPE1, and *CAT* after *FOXO1* silencing, suggesting that *FOXO1* promotes their transcription by binding to their promoters.

Previous literature has shown that SIRT1, as a deacetylase, can influence the transcriptional activity of FOXO1[42]. To assess the impact of SIRT1 on the activity of FOXO1 in AT2 cells, we evaluated the acetylation, phosphorylation, and cytoplasmic translocation of FOXO1. Compared to the PBS group, the LPS group exhibited a significant increase in the acetylation and phosphorylation levels of FOXO1 in AT2 cells (Fig. 5G), promoting the cytoplasmic translocation of FOXO1 (Fig. 5H) and subsequently inhibiting its transcriptional activity. However, after overexpressing SIRT1 (Fig. 5I), both acetylation and phosphorylation levels of FOXO1 significantly decreased (Fig. 5J), inhibiting the cytoplasmic-nuclear translocation of FOXO1 (Fig. 5K). This indicates that the deacetylase activity of SIRT1 on FOXO1 can inhibit its phosphorylation, thereby enhancing its transcriptional activity. Furthermore, in combination with ginsenoside Rb1 and the AMPK/SIRT1 pathway inhibitor Compound C treatment in AT2 cells, the results showed that Rb1 significantly reduced the acetylation and phosphorylation levels of FOXO1 (Fig. 5L), consequently inhibiting its cytoplasmic translocation (Fig. 5M). Treatment with Compound C reversed the above results.

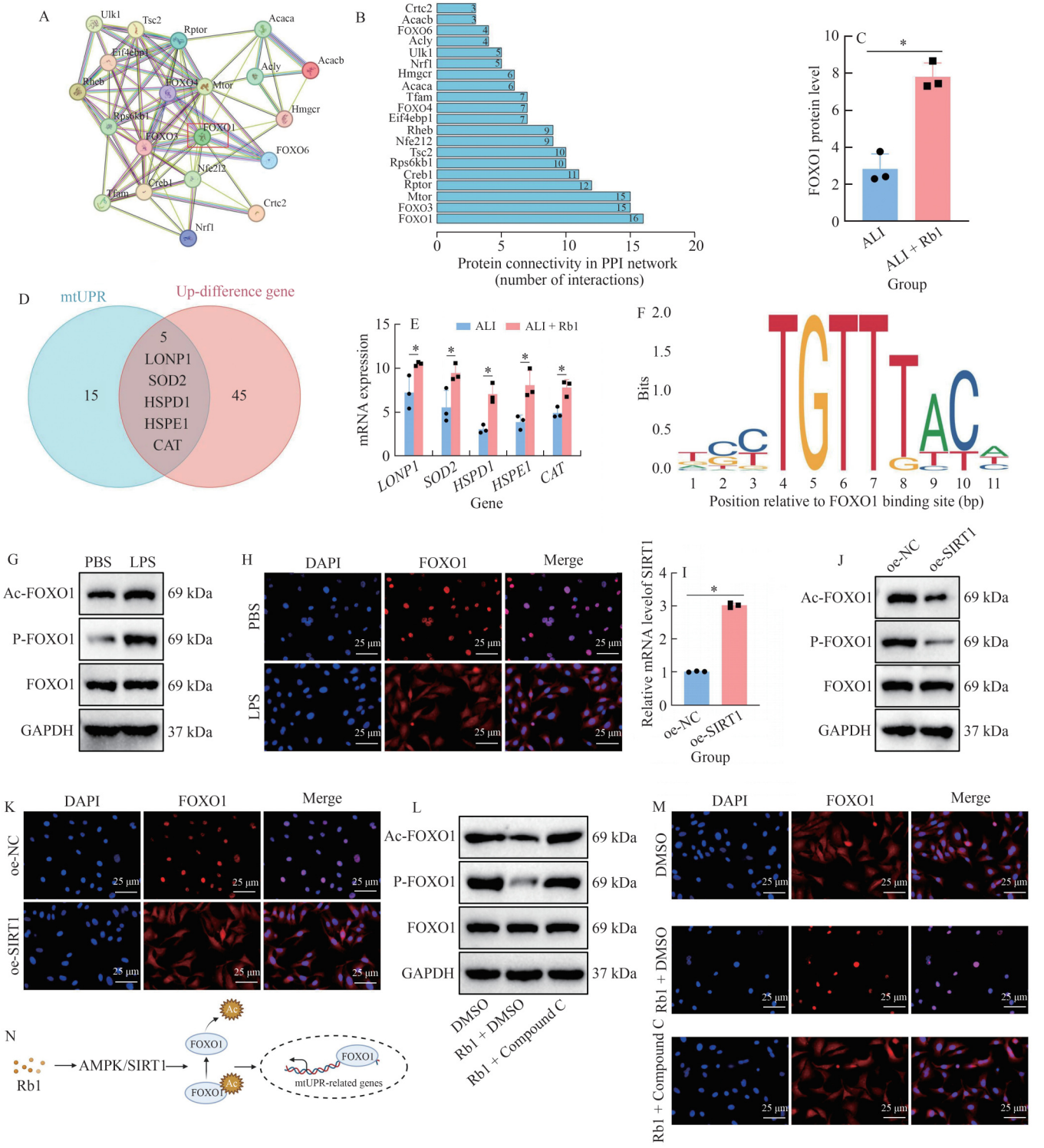

Fig. 5 Mechanistic insights of ginsenoside Rb1. (A) Construction of a PPI network based on the top 20 significantly upregulated proteins; (B) Column chart of core protein selection; (C) Protein expression of transcription factor FOXO1 in lung tissue proteomic sequencing; (D) Venn diagram showing the intersection of mtUPR-related genes with the top 50 significantly upregulated genes; (E) Expression levels of *LONP1*, *SOD2*, *HSPD1*, *HSPE1*, and *CAT* in lung tissue transcriptomic sequencing; (F) Transcription binding sites of FOXO1; (G) Western blot analysis of acetylation and phosphorylation levels of FOXO1 in cells post LPS-treated AT2; (H) Immunofluorescence detection of cytoplasmic translocation of FOXO1 in each cell group, scale bar = 25 μm; (I) RT-qPCR assessment of *SIRT1* expression levels in cells overexpressing SIRT1; (J) Changes in acetylation and phosphorylation levels of FOXO1 in cells overexpressing SIRT1, where Ac represents acetylation and P represents phosphorylation; (K) Immunofluorescence analysis of cytoplasmic translocation of FOXO1 in each cell group post SIRT1 overexpression, scale bar = 25 μm; (L) Detection of acetylation and phosphorylation levels of FOXO1 in cells treated with a combination of ginsenoside Rb1 and AMPK/SIRT1 pathway inhibitor Compound C in AT2 cells, where Ac represents acetylation and P represents phosphorylation; (M) Immunofluorescence assessment of cytoplasmic translocation of FOXO1 in each cell group following treatment with a combination of ginsenoside Rb1 and AMPK/SIRT1 pathway inhibitor Compound C in AT2 cells, scale bar = 25 μm; (N) Schematic illustration of the molecular mechanism by which Rb1 regulates FOXO1 through AMPK/SIRT1 pathway activation. *$P < 0.05$ when comparing 2 groups. All cellular experiments were replicated 3 times.

In conclusion, ginsenoside Rb1 can activate the AMPK/SIRT1 pathway to promote the deacetylation and nuclear translocation of FOXO1, activating the transcription of mtUPR-related genes (Fig. 5N).

3.5 Ginsenoside Rb1 improves LPS-induced mitochondrial damage in AT2 cells by regulating mtUPR through the AMPK/SIRT1 pathway and FOXO1

MtUPR is crucial in maintaining mitochondrial function and protecting cells from oxidative damage[42]. Investigating the impact of the AMPK/SIRT1 pathway and FOXO1 on mtUPR helps elucidate the mode of action of ginsenoside Rb1. We treated AT2 cells with a combination of ginsenoside Rb1 and the AMPK/SIRT1 pathway inhibitor Compound C and ginsenoside Rb1 and FOXO1 silencing. Experimental results showed that compared to the PBS group, in the LPS group, AT2 cells exhibited disrupted mitochondrial structure, increased punctate mitochondrial numbers, and severe mitochondrial fragmentation (Figs. S3A and B). Additionally, the mitochondrial fission gene mitochondrial fission 1 protein (*FIS1*) expression significantly increased, while the fusion gene optic atrophy 1 (*OPA1*) expression markedly decreased (Fig. S3C). Post-Rb1 treatment decreased the number of structurally disrupted mitochondria, with increased mitochondrial area and perimeter, preserving mitochondrial structural integrity. However, the protective effect of Rb1 on mitochondrial morphology was reversed by Compound C and sh-FOXO1 (Figs. 6A-C, S4A-C). MMP was assessed using JC-1 staining. The results indicated that compared to the PBS group, the MMP in AT2 cells of the LPS group significantly decreased, characterized by enhanced green fluorescence (Fig. S3D), signifying LPS-induced mitochondrial damage. Rb1 treatment restored the MMP, which was reversibly altered by Compound C and sh-FOXO1, counteracting the effect of Rb1 (Figs. 6D and S4D).

Using the mRFP-GFP-LC3 reporter system to monitor autophagic flux in AT2 cells, it was observed that in the PBS control group, autophagosomes were engulfed by lysosomes to form autolysosomes, as indicated by the high fluorescence intensity of "RFP-LC3 minus GFP-LC3", suggesting smooth autophagic flux. In AT2 cells treated with LPS, excessive autophagosomes (GFP-LC3) failed to be degraded in the acidic lysosomal environment, and the decreased fluorescence intensity of "RFP-LC3 minus GFP-LC3" indicated that autophagosomes could not fully mature into autolysosomes after LPS treatment (Fig. S3E). Treatment with Rb1 significantly enhanced the conversion of autophagosomes to autolysosomes, which could be reversed by Compound C and sh-FOXO1 (Figs. 6E and S4E). Cell and mitochondrial ROS levels were evaluated using DCFH-DA and MitoSOX, respectively. Rb1 treatment reduced the accumulation of ROS in the cells, and this effect was reversed by Compound C and sh-FOXO1, with a similar trend observed in mitochondrial ROS levels (Figs. 6F-G, S4F-G). Moreover, the analysis of mtUPR-related genes revealed a significant decrease in the expression levels of *LONP1*, *SOD2*, *HSPD1*, *HSPE1*, and *CAT* in LPS-treated AT2 cells compared to the PBS group (Fig. S3F). Rb1 treatment upregulated the expression of mtUPR-related genes, which could be reversed by Compound C and sh-FOXO1 (Figs. 6H, S4H).

In conclusion, Rb1 significantly ameliorated LPS-induced mitochondrial damage in AT2 cells by modulating the AMPK/SIRT1 pathway and FOXO1 expression. However, the protective effect of Rb1 could be reversed by inhibiting the AMPK/SIRT1 pathway with Compound C and silencing FOXO1, indicating the crucial roles of AMPK/SIRT1 and FOXO1 in the Rb1-mediated mtUPR.

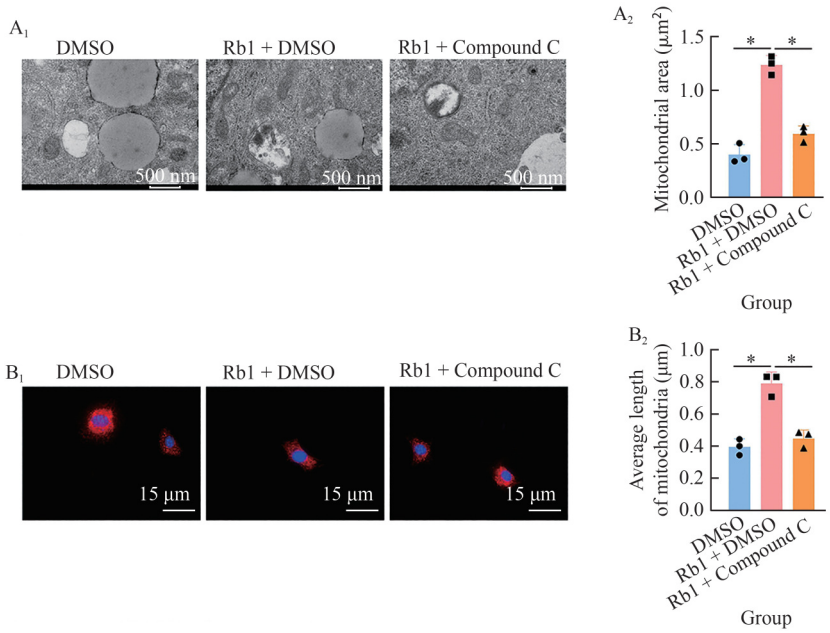

Fig. 6 Effects of AMPK/SIRT1 pathway inhibitors on ginsenoside rb1-mediated mtUPR. (A) TEM images depicting mitochondrial morphology in cells, scale bar = 500 nm; (B) Immunofluorescence analysis of mitochondrial morphology in various cell groups, with mitochondria marked in red and cell nuclei in blue, scale bar = 15 μm; (C) RT-qPCR assessment of expression levels of mitochondrial fission gene *FIS1* and fusion gene *OPA1* in cells from different groups; (D) JC-1 staining to evaluate MMP in various cell groups, scale bar = 25 μm; (E) Assessment of autophagic flux in different cell groups based on the mRFP-GFP-LC3 reporter system, scale bar = 15 μm; (F) DCFH-DA staining to detect ROS production in cells from different groups, scale bar = 25 μm; (G) Fluorescence images and corresponding quantitative data illustrating Mito-ROS MitoSOX fluorescence in cells from different groups, scale bar = 25 μm; (H) RT-qPCR analysis of *LONP1*, *SOD2*, *HSPD1*, *HSPE1*, and *CAT* expression levels in cells from various groups. **P* < 0.05, ***P* < 0.01, all cellular experiments were replicated 3 times.

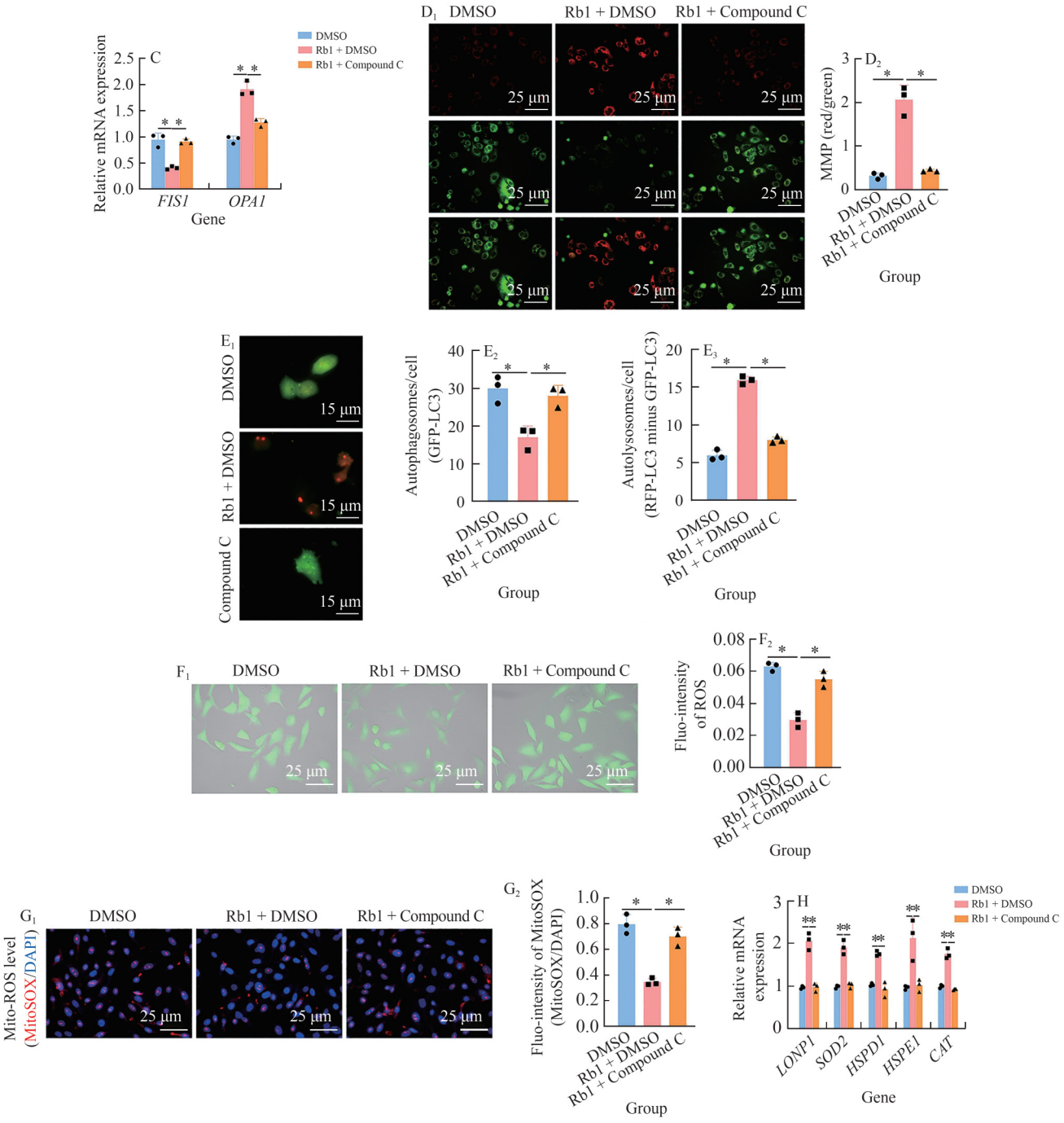

Fig. 6 (*Continued*)

3.6 Reversal of ginsenoside Rb1's impact on AT2 cell aging by inhibitors of the AMPK/SIRT1 pathway or FOXO1 silencing

In vitro, we further investigated the impact of Rb1 on AT2 cell aging by modulating the AMPK/SIRT1 pathway and FOXO1 expression. Our findings demonstrate that treatment with Rb1 significantly reduces the expression of pro-inflammatory genes in AT2 cells while increasing the activity of the antioxidant enzyme SOD. Moreover, both Compound C and sh-FOXO1 effectively reversed these changes (Figs. 7A-B, S5A-B). SA-β-gal staining revealed that Rb1 treatment prevents the aging of AT2 cells, a prevention that is reversed by Compound C and sh-FOXO1 interventions, as evidenced by a significant increase in *β*-galactosidase activity and a higher presence of aging-related blue staining in the cells (Figs. 7C and S5C). Furthermore, treatment with Compound C and sh-FOXO1 significantly upregulated the expression levels of aging-related markers such as *p16*, *p21*, and the pro-apoptotic gene *Bax*, while reducing the expression of the cell junction proteins *ZO-1*, *Occludin*, and *Claudin-3* (Figs. 7D-E, S5D-E).

In conclusion, the data illustrates that Rb1 can effectively alleviate the aging status of AT2 cells by modulating the AMPK/SIRT1 pathway and FOXO1 expression. This protective effect can be reversed by

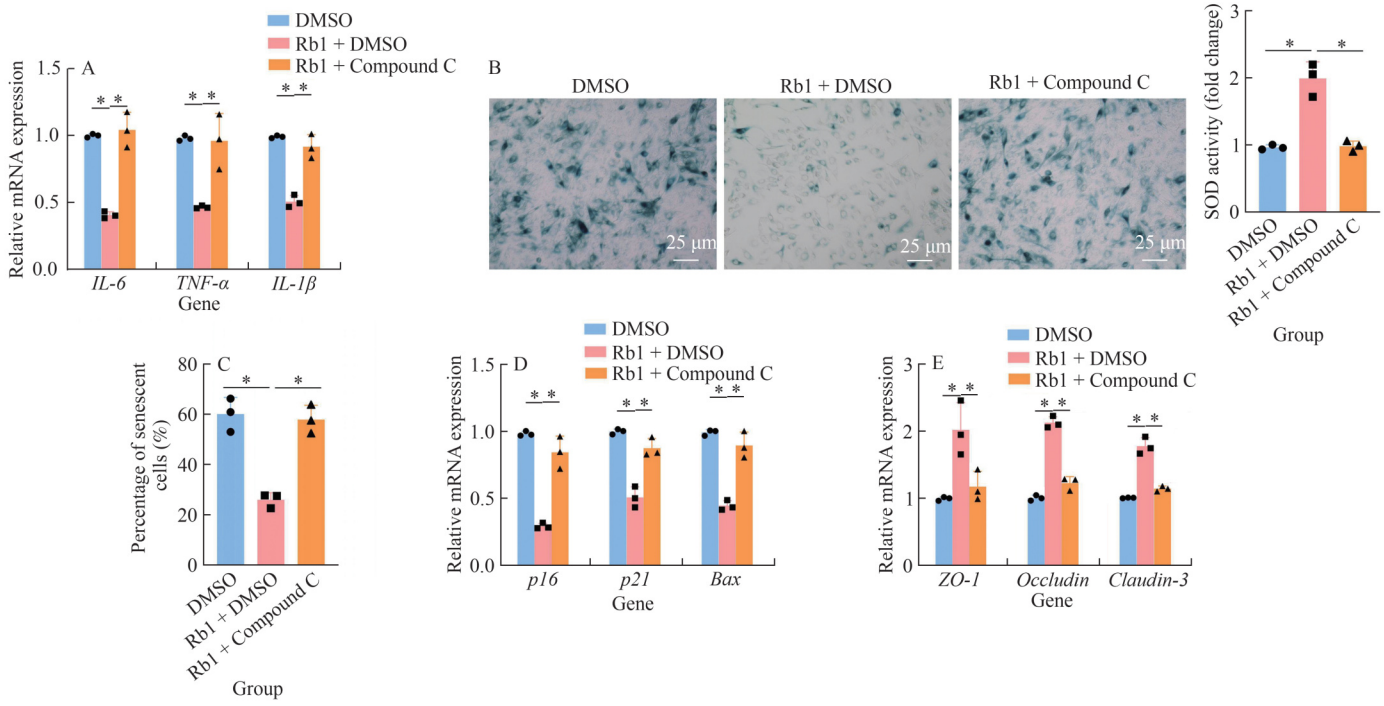

Fig. 7 Reversal of AMPK/SIRT1 pathway inhibitors on ginsenoside Rb1 induced senescence in AT2 cells. (A) RT-qPCR assessment of pro-inflammatory factor expression levels in cells from different groups; (B) SA-β-gal staining to evaluate the senescence status of AT2 cells in various groups, scale bar = 25 μm; (C) Measurement of SOD activity, an oxidative stress biomarker, in cells from different groups; (D) RT-qPCR analysis of the expression levels of senescence-related markers such as *p16*, *p21*, and apoptotic regulator *Bax* in cells from different groups; (E) RT-qPCR evaluation of the expression of junction markers *ZO-1*, *Occludin*, and *Claudin-3* in cells from different groups. *$P < 0.05$, all cellular experiments were repeated 3 times.

inhibitors of the AMPK/SIRT1 pathway and by silencing FOXO1.

3.7 Ginsenoside Rb1 improves sepsis-induced ALI by modulating the AMPK/SIRT1 pathway and FOXO1 expression

In this study, we further investigated the impact of Rb1 on sepsis-induced ALI *in vivo* by modulating the AMPK/SIRT1 pathway and FOXO1 expression. Initially, we treated ALI mice with different regimens. The results revealed that treatment with Rb1 significantly alleviated lung injury in mice, whereas Compound C and sh-FOXO1 reversed the protective effect of Rb1, leading to exacerbated lung injury characterized by thickened alveolar walls, increased inflammatory cell infiltration, worsened edema, and an elevated wet-to-dry lung weight ratio (Figs. 8A-B, S6A-B). Transmission electron microscopy (TEM) images displayed that following Rb1 treatment, mitochondrial fragmentation and cristae vacuolization in mouse lung tissues markedly decreased, indicating that Rb1 could ameliorate mitochondrial dysfunction, a protection that was reversed by Compound C and sh-FOXO1 (Figs. 8C and S6C). Evan's Blue and TUNEL staining revealed that post-Rb1 treatment, both the permeability of the pulmonary epithelial barrier and the rate of cell apoptosis in lung tissues significantly decreased. Similarly, Compound C and sh-FOXO1 reversed this effect (Figs. 8D-E, S6D-E).

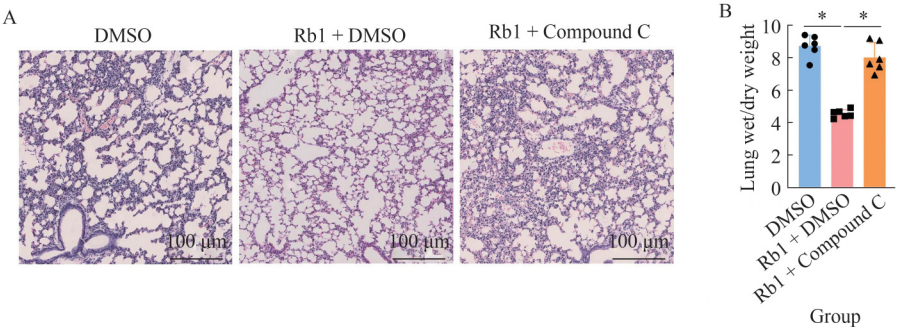

Fig. 8 Reversal of AMPK/SIRT1 pathway inhibitors on the effect of ginsenoside Rb1 on sepsis-induced ALI. (A) Histopathological changes in mouse lung tissues in each group assessed by H&E staining, scale bar = 100 μm; (B) Ratio of wet-to-dry weight of lung tissues in various mouse groups, shown in a statistical chart; (C) TEM images displaying mitochondria in mouse lung tissues in each group along with quantitative data on mitochondrial length and cristae density, scale bar = 2 μm; (D) Evaluation of lung epithelial barrier permeability in mice using Evan's Blue staining; (E) TUNEL staining to measure the apoptosis rate of lung tissue cells, scale bar = 100 μm; (F) ROS fluorescence staining images in mouse lung tissues from each group, scale bar = 100 μm; (G-H) Activity levels of oxidative stress markers TBARS and SOD in mouse lung tissues among different groups; (I) RT-qPCR analysis of pro-inflammatory factor expression levels in mouse lung tissues from each group. *$P < 0.05$ when comparing 2 groups, with 6 mice in each group.

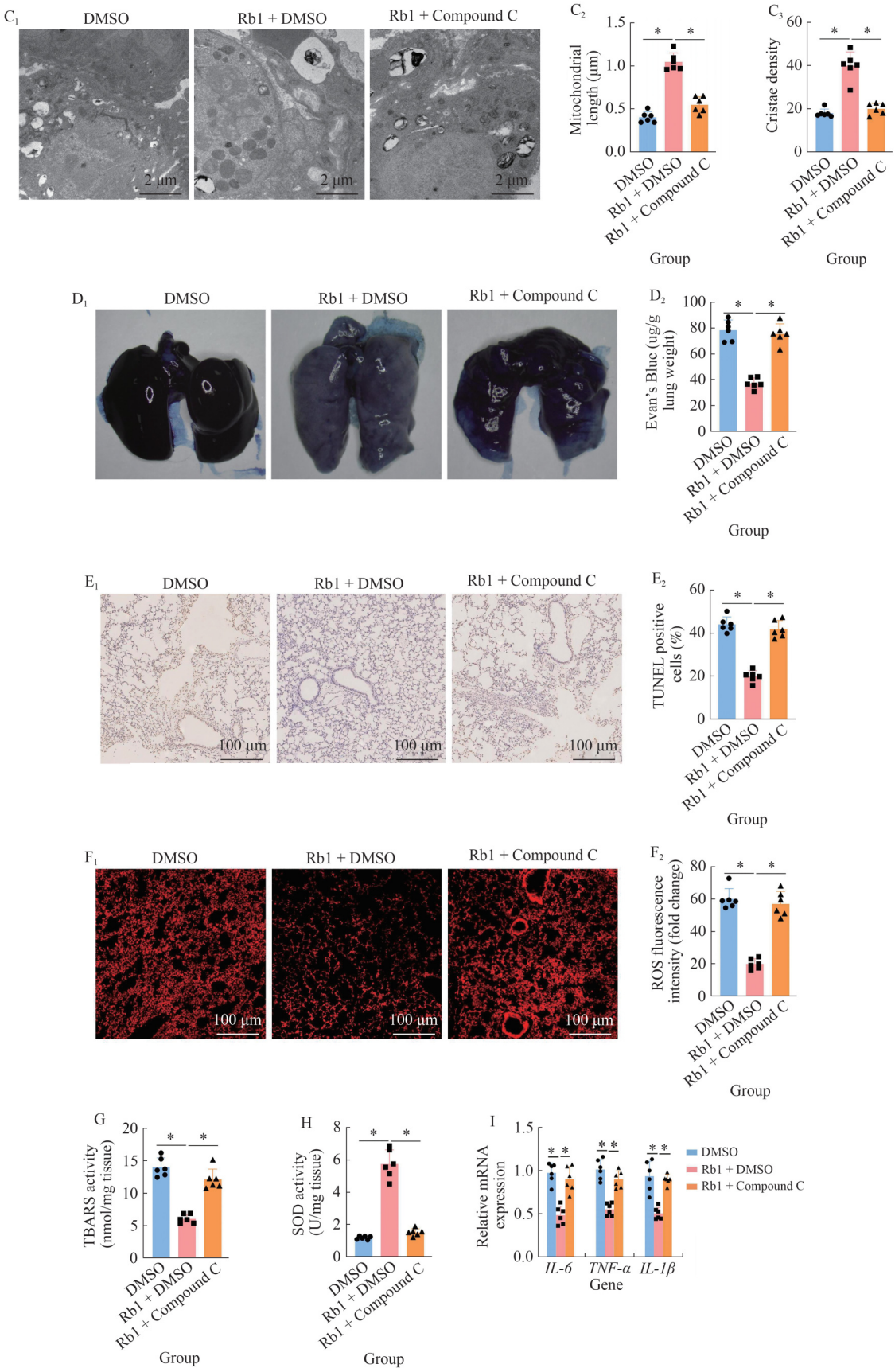

Fig. 8 (*Continued*)

Moreover, Rb1 treatment significantly inhibited oxidative stress and inflammatory responses in the lung tissues of ALI mice, while post-treatment with Compound C and sh-FOXO1 resulted in significantly elevated levels of oxidative stress markers ROS and TBARS activity, as well as reduced SOD activity. Additionally, there was a substantial increase in the expression of pro-inflammatory genes *IL-6*, *TNF-α*, and *IL-1β* in lung tissues post-Compound C and sh-FOXO1 treatment, indicating the reversal of Rb1's anti-inflammatory effect (Figs. 8F-I, S6F-I).

The findings indicate that Rb1 significantly improves sepsis-induced ALI by modulating the AMPK/SIRT1 pathway and FOXO1 expression. This protective effect can be reversed by inhibitors of the AMPK/SIRT1 pathway and by silencing FOXO1. This discovery provides crucial theoretical support for the therapeutic application of Rb1 in Sepsis-related lung injury and highlights the pivotal roles of the AMPK/SIRT1 pathway and FOXO1 in regulating lung tissue damage and inflammation.

4. Discussion

ALI is an acute inflammatory lung injury triggered by systemic infection, characterized by the destruction of alveolar epithelium and endothelial barriers, acute inflammatory response, oxidative stress, and cell apoptosis[1-2]. Despite various clinical treatment modalities, the prognosis for ALI patients remains unsatisfactory, with high mortality rates[3]. Therefore, searching for new therapeutic approaches, especially interventions based on natural products, is crucial[43-45]. This study focuses on ginsenoside Rb1, an active ingredient extracted from ginseng, which has demonstrated significant biological activity in various disease models. The aim of this research is to elucidate the specific mechanism by which ginsenoside Rb1 alleviates sepsis-induced ALI through the AMPK/SIRT1 signaling pathway, providing novel insights and strategies for ALI treatment.

Ginseng, as a traditional Chinese medicine, has attracted significant attention for the study of its active components. For instance, ferulic acid (FA) has been shown to inhibit colorectal cancer cells at different Duke's stages[46]. Research on ginsenoside Rb1 in various disease models has demonstrated its anti-inflammatory, antioxidant, and anti-tumor properties[47]. Previous studies on ginsenoside Rb1 have typically been limited to its applications. For example, Wu et al.[48] discovered that encapsulating ginsenoside Rb1 into biomimetic nanoparticles (R@ZQC npS) effectively reduced mitochondrial oxidative stress and inhibited apoptosis in alveolar macrophages. Other studies have focused on different pathways, such as the PGC-1α/Nrf2 signaling pathway[49]. In this study, it was found that ginsenoside Rb1 activates the AMPK/SIRT1 signaling pathway and regulates FOXO1 deacetylation and *mtUPR* gene transcription, thereby protecting AT2s from damage induced by sepsis-induced ALI. Unlike previous studies, this research uniquely used isotope tracing targeted metabolomics and proteomics techniques to systematically reveal the metabolic pathways and molecular mechanisms of Rb1 *in vivo*. While the protective role of the AMPK/SIRT1 signaling pathway has been widely reported in various pathological conditions. For example, in atherosclerosis and ischemia-reperfusion injury, this pathway exerts protective effects by regulating lipid metabolism, reducing inflammation, and preserving vascular endothelial function. In neurodegenerative diseases such as Alzheimer's and Parkinson's disease, it protects neurons from oxidative stress by enhancing protein clearance, reducing ROS levels, and mitigating inflammation[50]. Its specific mechanism of action in sepsis-induced ALI remains unclear. This study fills this research gap and provides new experimental evidence.

This study presents significant innovations in the analysis of metabolomics and proteomics. Using ^{13}C isotope-labeled Rb1 in conjunction with metabolomics analysis revealed that Rb1 metabolizes into F2 and CK *in vivo*, demonstrating anti-inflammatory effects. Previous studies have primarily focused on the direct effects of Rb1, neglecting the biological activities of its metabolites[51-53]. For the first time, this study systematically analyzed the effects of Rb1 and its metabolites in sepsis-induced ALI, offering a new perspective for further research on the pharmacological mechanisms of Rb1. Compared to traditional drug metabolism research methods, the isotope tracing technique employed in this study provides higher sensitivity and accuracy, enabling a more comprehensive elucidation of drug metabolism pathways and mechanisms.

This study extensively analyzed the deacetylation of FOXO1 and its impact on cellular senescence. FOXO1, a crucial transcription factor, exhibits significant functional variances depending on its localization in the nucleus and cytoplasm. It was found in this study that ginsenoside Rb1 activates the AMPK/SIRT1 signaling pathway, promoting the deacetylation of FOXO1, inhibiting its translocation to the cytoplasm, thereby activating the transcription of mtUPR-related genes to protect cells from aging and damage. Previous research has predominantly focused on the phosphorylation regulation of FOXO1, with relatively limited studies on its deacetylation. Through systematic experiments, this study validated the crucial role of FOXO1 deacetylation in sepsis-induced ALI, expanding our understanding of the regulatory mechanisms of FOXO1.

This study validated the mechanism of action of ginsenoside Rb1 through *in vitro* cell experiments and *in vivo* animal experiments. In the *in vitro* experiments, ginsenoside Rb1 significantly inhibited AT2 aging, displaying a clear anti-aging effect. Additionally, Rb1 notably improved mitochondrial function, restored MMP and reduced the generation of oxidative stress products. In the *in vivo* experiments, Rb1 effectively alleviated lung injury in sepsis-induced ALI mice, significantly reducing inflammation and apoptotic cell rates and diminishing pathological changes in lung tissue. The consistency of both results further confirms that Rb1 exerts a protective effect *via* the AMPK/SIRT1 signaling pathway, demonstrating its dual action at the molecular and systemic levels. Compared to prior research, a key innovation of this study lies in integrating multi-layered, multi-perspective experimental validations both *in vitro* and *in vivo*, rendering the research outcomes more persuasive and scientifically grounded, offering comprehensive evidence support.

The results of this study indicate that ginsenoside Rb1, by activating the AMPK/SIRT1 signaling pathway and regulating FOXO1 deacetylation, significantly mitigated lung injury in sepsis-induced ALI. Through this mechanism, Rb1 restored mitochondrial function, reduced oxidative stress, suppressed inflammation, and apoptotic cell death, ultimately improving lung function. This discovery presents new possibilities for clinical applications, especially considering ginsenoside Rb1 as a natural compound with multiple biological activities and relative safety, suggesting a broad potential scope of application. By elucidating its mechanism of action, this study lays a scientific foundation for using ginsenoside Rb1 in ALI treatment and provides a theoretical basis for developing new therapeutic drugs.

Future clinical research can further explore Rb1 dosage optimization, administration methods, and long-term safety to facilitate its clinical translation, offering a new, safe, and effective treatment option for ALI patients. Subsequent studies can also investigate the potential applications of Rb1 in other acute and chronic lung diseases, further expanding its clinical utility.

While this study has made significant progress, some limitations must be noted. The study primarily relied on mouse models and *in vitro* cell experiments. Although these results partly revealed the mechanism of action of ginsenoside Rb1, its actual effects on humans have not yet been validated. Additionally, we must point out that current animal models do not fully replicate the complexity of ALI. For example, although the LPS-induced ALI model used in this study is advantageous due to its ease of administration and high reproducibility[54], it cannot simulate the complex immune dysfunction and polymicrobial infection seen in human sepsis. Nevertheless, it remains a widely accepted model for dissecting inflammatory mechanisms and evaluating early-stage therapeutic effects in sepsis-related lung injury. Secondly, the study focused on the AMPK/SIRT1 signaling pathway without delving into other potential signaling pathways and their interactions, potentially limiting our comprehensive understanding of the mechanism of action of ginsenoside Rb1. Further research is needed to investigate the roles of Rb1 metabolites F2 and CK and their interactions with other cytokines. Lastly, the small sample size in the experiments suggests the need for larger-scale studies in the future to verify the universality and stability of these findings.

Future research directions in this field should be broader and more in-depth. This study focused on the central role of the AMPK/SIRT1 signaling pathway, but it is worth noting that ginsenoside Rb1 may exert its pharmacological effects through multiple targets. For example, nuclear factor kappa B (NF-κB) is a key regulator of the inflammatory response and has extensive cross-talk with the AMPK/SIRT1 pathway. Previous studies have shown that AMPK activation can block NF-κB nuclear translocation by inhibiting inhibitor of nuclear factor kappa-B kinase subunit beta (IKKβ) phosphorylation[55]. The observed reduction in inflammatory cytokines (e.g., TNF-α, IL-6) in this study may be partly due to the dual inhibition of the NF-κB pathway by AMPK/SIRT1. Future studies should employ ChIP assays or dual-luciferase reporter gene experiments to elucidate the dynamic regulation of NF-κB transcriptional activity by Rb1 and its metabolites. This would provide a more comprehensive understanding of the multi-pathway synergistic anti-inflammatory effects. Additionally, large-scale human clinical trials are needed to confirm the efficacy and safety of ginsenoside Rb1 in patients with sepsis-induced ALI, facilitating its clinical translation. Secondly, further exploration of the mechanism of action of Rb1 under different disease states, particularly its interactions with other signaling pathways, is essential to unveil the nature of its multiple biological activities. Thirdly, future research could explore the development of derivatives of Rb1 or the combination of these with other therapeutic approaches to enhance its therapeutic effects and bioavailability.

This study not only provides a novel therapeutic target for sepsis-induced ALI but also highlights the potential cross-disease applications of ginsenoside Rb1. Its core mechanism, coordinating mitochondrial repair and inflammation resolution through the AMPK/SIRT1 pathway, is broadly relevant in various pulmonary pathologies, including ARDS, chronic obstructive pulmonary disease (COPD), and idiopathic pulmonary fibrosis (IPF). We will continue to explore the potential applications of Rb1 in other acute and chronic lung diseases that could expand its clinical utility. Through multi-layered and multi-perspective research, it is hoped that the mechanism of action of ginsenoside Rb1 will be comprehensively elucidated, providing more effective and diversified strategies for clinical treatment.

5. Conclusion

Based on the comprehensive studies presented, we can preliminarily draw the following conclusions (Fig. 9): ginsenoside Rb1 can activate the AMPK/SIRT1 signaling pathway to facilitate FOXO1 deacetylation, thereby activating the transcription of mtUPR-related genes, preventing AT2 aging, and alleviating sepsis-induced ALI. Through the integration of advanced isotope tracing technology with metabolomics and proteomics analysis, this research delves into how ginsenoside Rb1 regulates the activity of AMPK/SIRT1

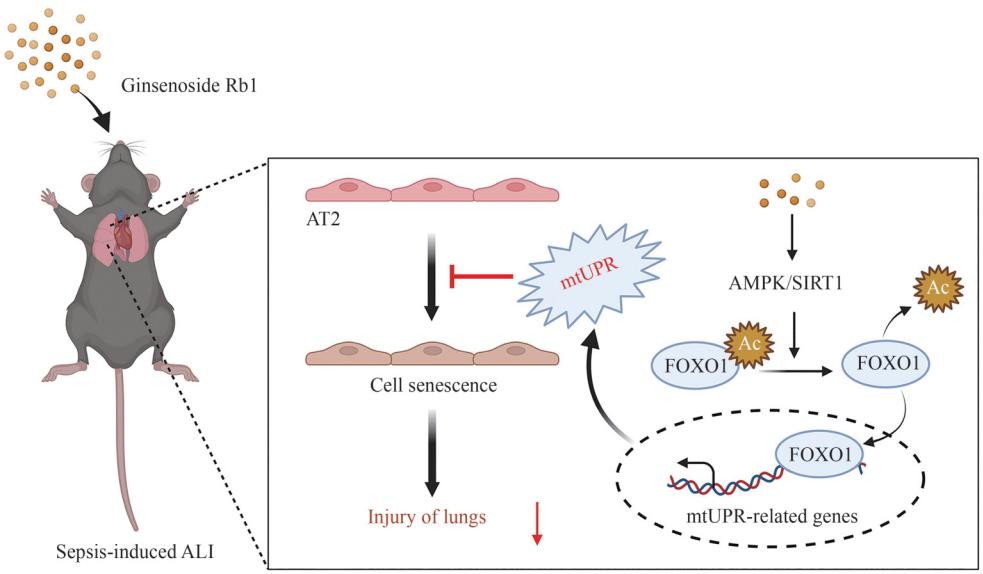

Fig. 9 Molecular mechanism of ginsenoside Rb1 prevents AT2 aging and alleviates ALI.

signaling pathways and FOXO1, inhibiting the aging of AT2s and promoting cell survival. This study provides new insights into understanding the complex mechanisms of plant medicines in regulating cell signaling pathways. Ginsenoside Rb1 demonstrates therapeutic potential in sepsis-induced ALI, which might offer a scientific basis for developing new drugs to treat sepsis and its complications. Furthermore, the study suggests the potential of slowing down cell aging and improving tissue damage through drug-induced activation of specific signaling pathways, which is important for delaying the development of age-related diseases. While mouse ALI models can partially mimic human disease states, the differences between mice and humans in immune responses and metabolic pathways may constrain the direct translation of research findings into applications. Long-term effects remain unclear. Additionally, the research mainly focuses on the short-term effects of ginsenoside Rb1 on ALI, indicating the necessity for further investigation into its long-term effects and safety profile.

Conflict of interest

The author declares no conflict of interest.

Acknowledgements

This work was supported by the High-Quality Development Projects of China Medical University, supported by the Science and Technology Bureau of Liaoning Province (2023JH2/20200121).

Data Availability

All data can be provided as needed.

Appendix A. Supplementary data

Supplementary data associated with this article can be found, in the online version, at http://doi.org/10.26599/FSHW.2025.9250658.

References

[1] K. Shen, X. Wang, Y. Wang, et al., miR-125b-5p in adipose derived stem cells exosome alleviates pulmonary microvascular endothelial cells ferroptosis *via* Keap1/Nrf2/GPX4 in sepsis lung injury, Redox Biol. 62 (2023) 102655. https://doi.org/10.1016/j.redox.2023.102655.

[2] S. Zou, H. Jie, X. Han, et al., The role of neutrophil extracellular traps in sepsis and sepsis-related acute lung injury, Int. Immunopharmacol. 124 (2023) 110436. https://doi.org/10.1016/j.intimp.2023.110436.

[3] F. Zheng, Y. Pan, Y. Yang, et al., Novel biomarkers for acute respiratory distress syndrome: genetics, epigenetics and transcriptomics, Biomark. Med. 16 (2022) 217-231. https://doi.org/10.2217/bmm-2021-0749.

[4] R.Q. Yao, Z. Shen, Q.M. Ma, et al., Combination of transcriptional biomarkers and clinical parameters for early prediction of sepsis indued acute respiratory distress syndrome, Front. Immunol. 13 (2023) 4568. https://doi.org/10.3389/fimmu.2022.1084568.

[5] P.F. Dequin, F. Meziani, J.P. Quenot, et al., Hydrocortisone in severe community-acquired pneumonia, N. Engl. J. Med. 388 (2023) 1931-1941. https://doi.org/10.1056/nejmoa2215145.

[6] G. Emeriaud, Y.M. López-Fernández, N.P. Iyer, et al., Executive summary of the second international guidelines for the diagnosis and management of pediatric acute respiratory distress syndrome (PALICC-2), Pediatric Critical Care Medicine 24 (2023) 143-168. https://doi.org/10.1097/pcc.0000000000003147.

[7] D. Mokrá, Acute lung injury-from pathophysiology to treatment, Physiol. Res. 69 (2020) S353-S366. https://doi.org/10.33549/physiolres.934602.

[8] Y. Wang, Y. Yuan, W. Wang, et al., Mechanisms underlying the therapeutic effects of Qingfeiyin in treating acute lung injury based on GEO datasets, network pharmacology and molecular docking, Comput. Biol. Med. 145 (2022) 105454. https://doi.org/10.1016/j.compbiomed.2022.105454.

[9] J. Li, K. Lu, F. Sun, et al., Panaxydol attenuates ferroptosis against LPS-induced acute lung injury in mice by Keap1-Nrf2/HO-1 pathway, J. Transl. Med. 19 (2021) 1-14. https://doi.org/10.1186/s12967-021-02745-1.

[10] Y. Wang, X. Wang, Y. Li, et al., Xuanfei Baidu Decoction reduces acute lung injury by regulating infiltration of neutrophils and macrophages *via* PD-1/IL17A pathway, Pharmacological Research 176 (2022) 106083. https://doi.org/10.1016/j.phrs.2022.106083.

[11] H. Zhu, S. Wang, C. Shan, et al., Mechanism of protective effect of Xuan-bai-cheng-qi decoction on LPS-induced acute lung injury based on an integrated network pharmacology and RNA-sequencing approach, Respir. Res. 22 (2021) 1-14. https://doi.org/10.1186/s12931-021-01781-1.

[12] S. Zhou, S. Lu, S. Guo, et al., Protective effect of ginsenoside Rb1 nanoparticles against contrast-induced nephropathy by inhibiting high mobility group box 1 gene/toll-like receptor 4/NF-κB signaling pathway, J. Biomed. Nanotechnol. 17 (2021) 2085-2098. https://doi.org/10.1166/jbn.2021.3163.

[13] Q. Zhang, J. Hu, A. Mao, et al., Ginsenoside Rb1 alleviated concanavalin A-induced hepatocyte pyroptosis by activating mitophagy, Food Funct. 14 (2023) 3793-3803. https://doi.org/10.1039/d2fo03130b.

[14] Y. Wang, J. Wu, Y. Hong, et al., Ginsenosides retard atherogenesis *via* remodelling host-microbiome metabolic homeostasis, British J. Pharmacology. 181 (2024) 1768-1792. https://doi.org/10.1111/bph.16320.

[15] J. Luan, G. Che, G. Man, et al., Ginsenoside Rb1 from *Panax ginseng* attenuates monoiodoacetate-induced osteoarthritis by inhibiting miR-21-5p/FGF18-mediated inflammation, J. Food Biochem. 46 (2022) 14340. https://doi.org/10.1111/jfbc.14340.

[16] S.S. Ahmad, H.J. Chun, K. Ahmad, et al., Therapeutic applications of ginseng for skeletal muscle-related disorder management, Journal of Ginseng Research 48 (2024) 12-19. https://doi.org/10.1016/j.jgr.2023.06.003.

[17] M. Zhang, W. Lin, X. Tao, et al., Ginsenoside Rb1 inhibits ferroptosis to ameliorate hypoxic-ischemic brain damage in neonatal rats, Int. Immunopharmacol. 121 (2023) 110503. https://doi.org/10.1016/j.intimp.2023.110503.

[18] X. Tang, X. Yang, Y. Yu, et al., Carbon quantum dots of ginsenoside Rb1 for application in a mouse model of intracerebral Hemorrhage, J. Nanobiotechnol. 22 (2024) 125. https://doi.org/10.1186/s12951-024-02368-w.

[19] H.S. Li, J.Y. Kuang, G.J. Liu, et al., Myostain is involved in ginsenoside Rb1-mediated anti-obesity, Pharm. Biol. 60 (2022) 1106-1115. https://doi.org/10.1080/13880209.2022.2074056.

[20] C. Li, X. Zhang, J. Li, et al., Ginsenoside Rb1 promotes the activation of PPARα pathway *via* inhibiting FADD to ameliorate heart failure, Eur. J. Pharmacol. 947 (2023) 175676. https://doi.org/10.1016/j.ejphar.2023.175676.

[21] U.M. Parmar, M.P. Jalgaonkar, Y.A. Kulkarni, et al., Autophagy-nutrient sensing pathways in diabetic complications, Pharmacol. Res. 184 (2022) 106408. https://doi.org/10.1016/j.phrs.2022.106408.

[22] S. Jiang, S. Liu, Y. Hou, et al., Cardiac-specific overexpression of Claudin-5 exerts protection against myocardial ischemia and reperfusion injury, Biochimica et Biophysica Acta 1868 (2022) 166535. https://doi.org/10.1016/j.bbadis.2022.166535.

[23] G.R. Steinberg, D.G. Hardie, New insights into activation and function of the AMPK, Nat. Rev. Mol. Cell Biol. 24 (2022) 255-272. https://doi.org/10.1038/s41580-022-00547-x.

[24] M. Aslam, Y. Ladilov, Emerging role of cAMP/AMPK signaling, Cells 11 (2022) 308. https://doi.org/10.3390/cells11020308.

[25] X. Wang, X. Tan, J. Zhang, et al., The emerging roles of MAPK-AMPK in ferroptosis regulatory network, Cell Commun. Signal. 21 (2023) 200. https://doi.org/10.1186/s12964-023-01170-9.

[26] Y. Xu, W. Wan, Acetylation in the regulation of autophagy, Autophagy 19 (2022) 379-387. https://doi.org/10.1080/15548627.2022.2062112.

[27] S. Kumariya, V. Ubba, R.K. Jha, et al., Autophagy in ovary and polycystic ovary syndrome: role, dispute and future perspective, Autophagy 17 (2021) 2706-2733. https://doi.org/10.1080/15548627.2021.1938914.

[28] Y. Feng, Y. Chen, X. Wu, et al., Interplay of energy metabolism and autophagy, Autophagy 20 (2023) 4-14. https://doi.org/10.1080/15548627.2023.2247300.

[29] Q. Ye, H. Xu, S. Liu, et al., Apoptotic extracellular vesicles alleviate Pg-LPS induced inflammatory responses of macrophages *via* AMPK/SIRT1/NF-κB pathway and inhibit osteoclast formation, J. Periodontol. 93 (2022) 1738-1751. https://doi.org/10.1002/jper.21-0657.

[30] J. Lü, Y. Li, S. Shi, et al., Skeletal muscle mitochondrial remodeling in heart failure: an update on mechanisms and therapeutic opportunities, Biomed. Pharmacother. 155 (2022) 113833. https://doi.org/10.1016/j.biopha.2022.113833.

[31] W. Xu, J. Yan, U. Ocak, et al., Melanocortin 1 receptor attenuates early brain injury following subarachnoid hemorrhage by controlling mitochondrial metabolism *via* AMPK/SIRT1/PGC-1α pathway in rats, Theranostics. 11 (2021) 522-539. https://doi.org/10.7150/thno.49426.

[32] X. Feng, X. Chen, M. Zaeem, et al., Sesamol attenuates neuroinflammation by regulating the AMPK/SIRT1/NF-κB signaling pathway after spinal cord injury in mice, Oxid. Med. Cell. Longev. 2022 (2022) 1-18. https://doi.org/10.1155/2022/8010670.

[33] Q. Yu, L. Zou, X. Yuan, et al., Dexmedetomidine protects against septic liver injury by enhancing autophagy through activation of the AMPK/SIRT1 signaling pathway, Front. Pharmacol. 12 (2021) 658677. https://doi.org/10.3389/fphar.2021.658677.

[34] C. Guo, Q. Huang, Y. Wang, et al., Therapeutic application of natural products: NAD^+ metabolism as potential target, Phytomedicine 114 (2023) 154768. https://doi.org/10.1016/j.phymed.2023.154768.

[35] X. Zhang, L. Wang, R. Guo, et al., Ginsenoside Rb1 ameliorates diabetic arterial stiffening *via* AMPK pathway, Front. Pharmacol. 12 (2021) 753881. https://doi.org/10.3389/fphar.2021.753881.

[36] T. Qin, D. Feng, B. Zhou, et al., Melatonin suppresses LPS-induced oxidative stress in dendritic cells for inflammatory regulation *via* the Nrf2/HO-1 axis, Antioxidants 11 (2022) 2012. https://doi.org/10.3390/antiox11102012.

[37] H. Su, C.J. Tian, Y. Wang, et al., Ginsenoside Rb1 reduces oxidative/carbonyl stress damage and ameliorates inflammation in the lung of streptozotocin-induced diabetic rats, Pharm. Biol. 60 (2022) 2229-2236. https://doi. org/10.1080/13880209.2022.2140168.

[38] N. Li, B. Liu, R. Xiong, et al., HDAC3 deficiency protects against acute lung injury by maintaining epithelial barrier integrity through preserving mitochondrial quality control, Redox Biol. 63 (2023) 102746. https://doi. org/10.1016/j.redox.2023.102746.

[39] W.Y. Yu, C.X. Gao, H.H. Zhang, et al., Herbal active ingredients: potential for the prevention and treatment of acute lung injury, BioMed Res. Int. 2021 (2021) 3185. https://doi.org/10.1155/2021/5543185.

[40] M. Lehmann, Q. Hu, Y. Hu, et al., Chronic WNT/*β*-catenin signaling induces cellular senescence in lung epithelial cells, Cell. Signal. 70 (2020) 109588. https://doi.org/10.1016/j.cellsig.2020.109588.

[41] H. Weng, Y. Ma, L. Chen, et al., A new vision of mitochondrial unfolded protein response to the sirtuin family, Curr. Neuropharmacol. 18 (2020) 613-623. https://doi.org/10.2174/1570159x18666200123165002.

[42] P. Cilleros-Holgado, D. Gómez-Fernández, R. Piñero-Pérez, et al., mtUPR modulation as a therapeutic target for primary and secondary mitochondrial diseases, IJMS 24 (2023) 1482. https://doi.org/10.3390/ijms24021482.

[43] L. Evans, A. Rhodes, W. Alhazzani, et al., Surviving sepsis campaign: international guidelines for management of sepsis and septic shock 2021, Intensive Care Med. 47 (2021) 1181-1247. https://doi.org/10.1007/s00134-021-06506-y.

[44] J. Song, X. Fang, K. Zhou, et al., Sepsis-induced cardiac dysfunction and pathogenetic mechanisms (review), Mol. Med. Rep. 28 (2023) 13114. https://doi.org/10.3892/mmr.2023.13114.

[45] J.E. Sevransky, R.E. Rothman, D.N. Hager, et al., Effect of vitamin C, thiamine, and hydrocortisone on ventilator- and vasopressor-free days in patients with sepsis, JAMA 325 (2021) 742. https://doi.org/10.1001/jama.2020.24505.

[46] Z.P. Liu, W.S. Tang, G.Z. Wang, et al., Ferulic acid inhibiting colon cancer cells at different Duke's stages, Food Medicine Homology 1 (2025) 9420063. https://doi.org/10.26599/fmh.2025.9420063.

[47] F. Yao, J. Yang, Y. Huang, et al., Antinociceptive effects of ginsenoside Rb1 in a rat model of cancer-induced bone pain, Exp. Ther. Med. 2019 (2019) 7404. https://doi.org/10.3892/etm.2019.7404.

[48] S. Wu, H. Liu, X. Liu, et al., Ginsenoside Rb1-loaded bionic nanoparticles alleviate sepsis-induced acute lung injury by reducing mitochondrial oxidative stress to inhibit macrophage PANoptosis, Mater. Des. 245 (2024) 113291. https://doi.org/10.1016/j.matdes.2024.113291.

[49] R. Liu, Q. Wang, Y. Li, et al., Ginsenoside Rg1 alleviates sepsis-induced acute lung injury by reducing FBXO3 stability in an m6A-dependent manner to activate PGC-1α/Nrf2 signaling pathway, AAPS J. 26 (2024). https://doi.org/10.1208/s12248-024-00919-5.

[50] G. Guan, Y. Chen, Y. Dong, Unraveling the AMPK-SIRT1-FOXO pathway: the in-depth analysis and breakthrough prospects of oxidative stress-induced diseases, Antioxidants 14 (2025) 70. https://doi.org/10.3390/antiox14010070.

[51] T. Yu, Y. Tang, F. Zhang, et al., Roles of ginsenosides in sepsis, J. Ginseng Res. 47 (2023) 1-8. https://doi.org/10.1016/j.jgr.2022.05.004.

[52] L. Lu, H. Ao, J. Fu, et al., Ginsenoside Rb1 stabilized and paclitaxel/protopanaxadiol co-loaded nanoparticles for synergistic treatment of breast tumor, Biomedicine Pharmacotherapy 163 (2023) 114870. https://doi.org/10.1016/j.biopha.2023.114870.

[53] V. Serra, A.T. Wang, M. Castroviejo-Bermejo, et al., Identification of a molecularly-defined subset of breast and ovarian cancer models that respond to WEE1 or ATR inhibition, overcoming PARP inhibitor resistance, Clin. Cancer Res. 28 (2022) 4536-4550. https://doi.org/10.1158/1078-0432.ccr-22-0568.

[54] Y. Shen, Y. He, Y. Pan, et al., Role and mechanisms of autophagy, ferroptosis, and pyroptosis in sepsis-induced acute lung injury, Front. Pharmacol. 15 (2024) 5145. https://doi.org/10.3389/fphar.2024.1415145.

[55] D. Lee, J.Y. Imm, AMP kinase activation and inhibition of nuclear factor-kappa B (NF-κB) translocation contribute to the anti-inflammatory effect of tricin, J. Food Biochem. 41 (2016) e12293. https://doi.org/10.1111/jfbc.12293.